Available online at www.sciencedirect.com
ScienceDirect
Trans. Nonferrous Met. Soc. China 33(2023) 2183−2205
Transactions of Nonferrous Metals Society of China
www.tnmsc.cn

Experiment and thermodynamic modelling of phase equilibria in PbO−"$CuO_{0.5}$" and PbO−"$CuO_{0.5}$"−"$FeO_{1.5}$" slag systems with metal

X. WEN, M. SHEVCHENKO, E. JAK

Pyrometallurgy Innovation Centre (PYROSEARCH), School of Chemical Engineering, The University of Queensland, Brisbane, QLD 4072, Australia

Received 31 March 2022; accepted 20 September 2022

Abstract: The phase equilibria of the PbO−"$CuO_{0.5}$" and PbO−"$CuO_{0.5}$"−"$FeO_{1.5}$" slag systems in equilibrium with solid metallic copper and/or liquid metallic lead−copper alloy were studied as part of the investigation of the 19-element PbO−ZnO−Cu_2O−FeO−Fe_2O_3−CaO−SiO_2−Al_2O_3−MgO−S−(As, Sn, Sb, Bi, Ag, Au, Ni, Cr, Co as minor elements) multicomponent slag/matte/metal/speiss system, supporting the operation and development of the existing and emerging pyrometallurgical processes. In the experimental portion of this study, samples underwent high temperature equilibration followed by quenching, after which the compositions in the liquid slag, solid oxide and metallic phases were directly measured by electron probe microanalysis (EPMA). Phase equilibria data on the massicot (PbO), spinel ((Fe,Cu)Fe_2O_4), cuprite (Cu_2O), lead ferrite ($Pb_{2+x}Fe_2O_{5+x}$), magnetoplumbite ($Pb_{1+x}Fe_{12-x}O_{19-x}$), copper plumbite ($Cu_2PbO_2$), and delafossite ($CuFeO_2$) primary phase fields were obtained between 688 and 1000 °C. A key finding of the experimental study of the PbO−"$CuO_{0.5}$" subsystem was that the copper plumbite (Cu_2PbO_2) phase melted incongruently, contradicting previous studies that suggested it apparently decomposed below the binary eutectic temperature to form massicot (PbO) and cuprite (Cu_2O). Based on the results of past and present experimental studies, a self-consistent set of thermodynamic model parameters describing all phases in the system was derived using the FactSage software package.

Key words: lead oxide; copper oxide; iron oxide; phase diagram; liquidus; slag; metal; phase equilibrium

1 Introduction

A combination of resource depletion and the need to treat complex secondary feedstocks (e.g., waste from electrical and electronic equipment) has led to closer integration of the copper−lead−zinc production processes and increases in the complexity of the process chemistry [1−3]. In lead smelting, the use of lead-bearing materials from adjacent copper smelters such as slimes, dusts, and copper−lead matte leads to elevated Cu throughput [3]. Likewise in copper smelting, there have been increased levels of Pb throughput, evidenced by the increased lead concentration in copper anodes found by a recent global survey of copper smelter practice [4]. The development of new processes and the optimization of existing processes require computational tools capable of predicting the partitioning of all elements, phase equilibria and energy balance. In turn, the accuracy of the predictions is improved by the integrated experimental and thermodynamic modelling study.

The present study is focused on the phase equilibria, in particular the liquidi, of the PbO−"$CuO_{0.5}$" and PbO−"$CuO_{0.5}$"−"$FeO_{1.5}$" slag systems in equilibrium with solid metallic copper and/or Pb−Cu liquid alloy. These systems are important for

Corresponding author: X. WEN, E-mail: x.wen@uq.edu.au
DOI: 10.1016/S1003-6326(23)66252-1

the lead and copper smelting, converting, and recycling processes, which involve slags that may contain all three oxides as major elements. The study is part of a broader research program to characterize the chemical behavior of the 19-element PbO−ZnO−Cu_2O−FeO−Fe_2O_3−CaO−SiO_2−Al_2O_3−MgO−S−(As, Sn, Sb, Bi, Ag, Au, Ni, Cr, and Co as minor elements) multicomponent system for the nonferrous metal smelting and recycling industries. The experimental data were used in the development of the thermodynamic database describing this complex, multi-component system based on the use of the FactSage computer package [5].

A number of experimental and thermodynamic modelling studies of the phase equilibria of the PbO−"$FeO_{1.5}$", PbO−"$CuO_{0.5}$" and "$CuO_{0.5}$"−"$FeO_{1.5}$" pseudo-binary systems in equilibrium with metal using a variety of experimental techniques have been reported [6−18]. However, further information is required to accurately characterize the PbO−"$CuO_{0.5}$" and PbO−"$CuO_{0.5}$"−"$FeO_{1.5}$" slag systems.

In the only prior study of the PbO−"$FeO_{1.5}$" system in equilibrium with metallic lead found in literature, SHEVCHENKO and JAK [6] experimentally investigated the massicot (PbO), spinel (Fe_3O_4), and lead ferrite ($Pb_{2+x}Fe_2O_{5+x}$) primary phase fields between 770 and 1100 °C, and 50−90 mol.% PbO in the liquid slag, using the equilibration/quenching/electron probe X-ray microanalysis (EPMA) technique with magnetite (Fe_3O_4) or iridium substrates. Based on the experimental data obtained, SHEVCHENKO and JAK [7] developed the thermodynamic description of the system. The spinel (Fe_3O_4) phase was experimentally found to contain up to 2 mol.% PbO, however, this was not described in the thermo-dynamic model developed.

SHEVCHENKO and JAK [12] reviewed the PbO−"$CuO_{0.5}$" system in equilibrium with metal as part of the experimental study of the PbO−"$CuO_{0.5}$"−SiO_2 system in equilibrium with metal, finding experimental data [8−11] in the range of 100−1250 °C and the entire range of liquid slag compositions. SHEVCHENKO and JAK [12] investigated the PbO−"$CuO_{0.5}$" system in the range of 730−950 °C and 30−80 mol.% PbO in the liquid slag, using the equilibration/quenching/EPMA technique with copper substrates to study the liquidi of the massicot (PbO) and cuprite (Cu_2O) primary phase fields in the range of 750−950 °C. Additionally, a sample was melted, and then recrystallized in Cu foil at 730 °C, resulting in a liquid slag-free mixture of massicot (PbO), copper plumbite (Cu_2PbO_2), and solid metallic copper, thereby defining the lower limit on the solidus temperature of the system. The previous studies have poor agreement on liquidus temperatures and compositions, and the reported peritectic temperature of copper plumbite (Cu_2PbO_2) [8−12]. The more recent results by SHEVCHENKO and JAK [12] are considered to be more accurate than the earlier studies [8−11], because (1) the liquid slag composition was directly measured after equilibration, and (2) the copper substrate used does not cross-contaminate the PbO−"$CuO_{0.5}$" slag, unlike the clay crucibles [8,9] and the quartz (SiO_2) tubes [10,11] used in the earlier studies. Based on the experimental data from the study by SHEVCHENKO and JAK [12], the thermodynamic description of the system was developed by SHEVCHENKO and JAK [13]; however, the eutectic temperature predicted by the model was noted to be inconsistent with the experimental results in that the experimentally determined solidus temperature (>730 °C) was higher than the thermodynamically assessed eutectic point of the system (720 °C).

The experimental studies of phase equilibria for the "$CuO_{0.5}$"−"FeO_x" system in equilibrium with metallic copper were found between the cuprite (Cu_2O)/delafossite ($CuFeO_2$) eutectic point (modelled to be 1128 °C by HIDAYAT et al [18]) and 1400 °C. YAZAWA and EGUCHI [14] investigated the "$CuO_{0.5}$"−"FeO_x" system in the range of 1150−1300 °C, and 0−45 mol.% "FeO_x" in the slag, using platinum substrates for all experiments. Differential thermal analysis (DTA) was used to investigate the spinel ((Fe,Cu)Fe_2O_4), cuprite (Cu_2O), and delafossite ($CuFeO_2$) primary phase fields up to a maximum of 1275 °C, while the equilibration/quenching/wet chemical analysis technique was used to determine the oxygen isobars for isothermal sections of the Cu−Fe−O diagram at 1200, 1250 and 1300 °C. TAKEDA [15] investigated the primary phase fields of the "$CuO_{0.5}$"−"FeO_x" system in the range of 1100−

1400 °C and 0−30 mol.% "FeO_x" in the slag, using a mixture of thermal analysis and equilibration/quenching/wet chemical analysis on magnesia (MgO) crucibles. ILYUSHECHKIN et al [16] and NIKOLIC et al [17] applied the equilibration/quenching/EPMA technique with the magnetite substrates to investigate the primary phase fields of the "$CuO_{0.5}$"−"FeO_x" system in equilibrium with metallic copper in the temperature range of 1150−1250 °C. The results by YAZAWA and EGUCHI [14] in the temperature range of 1100−1250 °C demonstrated poor agreement with those of TAKEDA [15], but good agreement with the later studies [16,17]. This is likely because in the study by TAKEDA [15], the liquid slag and the spinel ($(Fe,Mg,Cu)Fe_2O_4$) contained up to 1 and 16 wt.% MgO, respectively. A thermodynamic model description of the system was developed by HIDAYAT et al [18] using the data by YAZAWA and EGUCHI [14], ILYUSHECHKIN et al [16], and NIKOLIC et al [17].

No published phase equilibria data were available on the PbO−"$CuO_{0.5}$"−"$FeO_{1.5}$" system in equilibrium with solid metallic copper and/or the liquid metallic lead−copper alloy.

The present study addresses the inconsistency of information on the PbO−"$CuO_{0.5}$" system in equilibrium with solid metallic copper, and the lack of experimental phase equilibria data for the PbO−"$CuO_{0.5}$"−"$FeO_{1.5}$" slags in equilibrium with solid metallic copper and/or the liquid metallic lead−copper alloy.

2 Experimental

2.1 Experimental and analysis technique

The experimental/analytical techniques and equipment used in the present study were described in detail in previous publications [19,20]. In brief, the starting mixtures were made from high purity powders of PbO (≥99.9 wt.% in purity) and Cu_2O (≥99.9 wt.% in purity) supplied by Alfa-Aesar, MA, USA, and Fe_2O_3 (≥99.9 wt.% in purity) and "FeO" (≥99.9 wt.% in purity) supplied by Sigma-Aldrich, MO, USA. The mixtures were planned with the goal of obtaining a solid oxide fraction of about 10 vol.% to achieve equilibration and adequate outcomes from quenching (it was found that the distance between the solid phases should exceed 10−20 μm to ensure that the liquid slag is amorphous and uniform in composition). A 10−20 wt.% excess of Cu powder (≥99.9 wt.% in purity) supplied by Alfa Aesar, MA, USA, or Pb powder (≥99.9 wt.% in purity) supplied by Sigma-Aldrich, MO, USA was added to each oxide mixture to ensure that the quenched samples contained solid metallic copper and/or liquid metallic copper−lead alloy.

Less than 0.5 g of mixture was used in each equilibration experiment. The mixtures were pressed into pellets using a tool steel die before being placed on substrates. All experiments were performed on copper foil substrates (supplied by BDH Chemical Company, Poole, United Kingdom), or magnetite substrates (Fe_3O_4, prepared by oxidizing 99.9 wt.% pure Fe foil supplied by Sigma-Aldrich, MO, USA in 99.9% pure CO_2 supplied by Coregas, New South Wales, Australia at 1200 °C).

The high temperature equilibration experiments were performed in a vertical tube resistance-heated furnace. The reaction tube was made from impervious recrystallized alumina (Al_2O_3) with inner diameter of 30 mm (supplied by the Xiamen Wintrustek Advanced Materials Company, Fujian, China). To ensure that the sample was equilibrated at the correct temperature, an R-type reference thermocouple (previously calibrated against a standard thermocouple supplied by the National Measurement Institute of Australia, New South Wales, Australia) was inserted into the hot zone both prior to, and after sample equilibration (lead evaporated during equilibration can damage the thermocouple in inert or reducing atmospheres by forming Pb−Pt alloys). The overall temperature accuracies of the experiments were estimated to be ±3 K.

The samples were suspended in the hot zone of the furnace by copper wire (supplied by Goodfellow Cambridge Ltd., London, England), or Kanthal-D wire (Fe−Al−Cr alloy, supplied by Vulcan Stainless, Victoria, Australia). Argon or 0.3% CO in Ar (each 99.995% in purity, supplied by Coregas, New South Wales, Australia) was passed through the furnace during equilibration to prevent metal oxidation.

The samples were first pre-melted for 10−30 min at 20−130 °C above the final equilibration

temperature to form a homogeneous liquid slag + metal mixture. When a peritectic reaction was anticipated upon cooling the sample, the sample was also pre-cooled to 5−20 °C below the final equilibration temperature for 5−10 min following the pre-heating to facilitate the nucleation of the equilibrium solid oxide phases. Following equilibration, the samples were quenched into 30% $CaCl_2$ brine at −20 °C, washed using water and ethanol, dried in a convection oven at 40 °C, and then mounted in epoxy resin and cross-sectioned using conventional metallographic polishing techniques.

The cross-sectioned samples were examined under the optical microscope, carbon-coated, and then the compositions of the phases were measured using an electron probe X-ray microanalyser (JEOL 8200L EPMA; Japan Electron Optics Ltd., Tokyo, Japan) with the wavelength-dispersive spectrometer. The microanalyser was operated with 15 kV accelerating voltage and 20 nA probe current. The Duncumb-Philibert atomic number, absorption, and fluorescence (ZAF) correction supplied by JEOL [21−23] was applied. Copper (Cu) and hematite (Fe_2O_3) (supplied by the Charles M. Taylor Co., CA, USA), and K-456 lead silica glass (71.4 wt.% PbO, supplied by NIST, MD, USA) were used as EPMA standards. The concentrations of the metal cations were measured using EPMA: no data on the oxidation state of metal cations were obtained. For presentation purposes, the copper oxide concentration was re-calculated using the molecular mass and ZAF correction factor of "$CuO_{0.5}$" (as Cu^+ is the predominant copper cation in liquid slag in equilibrium with Cu metal [24]), and the iron oxide concentration was re-calculated using the molecular mass and ZAF correction factor of "$FeO_{1.5}$". The molar ratios of the oxides were used in the representation of the data.

For accurate, repeatable, and objective measurement of the average composition of the liquid slag phase, an approach similar to that described by NIKOLIC et al [25] was used during EPMA. The liquid slag composition was taken to be the average of 20 points in the best quenched area (usually near the slag/crucible interface), and the results were rejected if the standard deviation in the measured concentration of any metallic cation in the liquid slag exceeded 1 mol.%.

2.2 Custom correction of standard JEOL ZAF correction of measurements made using K_α and M_α X-rays

The accuracies of the EPMA compositional measurements made using K_α X-rays for Fe and Cu and M_α X-rays for Pb were improved by applying secondary corrections to concentrations obtained after applying the standard ZAF correction supplied by JEOL [21−23], following an approach similar to that described in previous publications by the authors [12]. The composition of the stochiometric copper plumbite (Cu_2PbO_2) phase present in equilibrated samples was measured using EPMA in a previous study [12]. It was found that after the application of the standard JEOL ZAF corrections, the concentration of "$CuO_{0.5}$" in copper plumbite (Cu_2PbO_2) was systematically overestimated by 0.8 mol.%, leading to copper plumbite (Cu_2PbO_2) being reported as containing 67.4 mol.% PbO rather than the expected 66.67 mol.%. Based on this reference point, the following correction factors were developed:

$$x_{CuO_{0.5}}^{Corrected} = x_{CuO_{0.5}}\left(1-3.36\times10^{-2}x_{PbO}\right) \quad (1)$$

$$x_{FeO_{1.5}}^{Corrected} = x_{FeO_{1.5}} \quad (2)$$

$$x_{PbO}^{Corrected} = 1 - x_{CuO_{0.5}}^{Corrected} - x_{FeO_{1.5}}^{Corrected} \quad (3)$$

where x_i refers to the normalised molar fractions of each component after the initial standard JEOL ZAF corrections, and $x_i^{Corrected}$ refers to the corrected, normalised molar fraction of each component. When the equations are applied to the Cu or Pb free sample, the corrected composition is equal to the composition after standard JEOL ZAF corrections only. When applied to copper plumbite (Cu_2PbO_2), its composition is corrected to 33.3 mol.% $CuO_{0.5}$ and 66.7 mol.% PbO (within the measurement uncertainty of the EPMA).

No suitable compounds were identified for developing similar correction factors for the PbO−"$FeO_{1.5}$" subsystem, because the lead ferrite ($Pb_{2+x}Fe_2O_{5+x}$) and magnetoplumbite ($Pb_{1+x}Fe_{12-x}O_{19-x}$) phases are not stoichiometric. Additional correction factors were not needed for "$CuO_{0.5}$"−"$FeO_{1.5}$" subsystem, because delafossite ($CuFeO_2$) was measured to have a "$CuO_{0.5}$" to "$FeO_{1.5}$" molar ratio of 1:1 within the measurement uncertainty of EPMA, and therefore the correct stoichiometry.

2.3 Composition measurements made using L_α X-rays

Both characteristic X-rays and background radiation (Bremsstrahlung) produced during EPMA can result in the generation of secondary X-rays and indirectly excite atoms adjacent to the material being measured by the probe. The concentrations of impurities in various phases may be overestimated by the EPMA measurements due to the generation of these secondary fluorescent X-rays [26]. Previous publications by the authors [12,27,28] demonstrated that the Cu, Fe and Zn concentrations in the SiO_2 solids could be overestimated by the EPMA measurements by up to 1−1.5 mol.%; when measured using K_α X-rays, nonzero Cu, Fe and Zn apparent concentrations were reported in 10−100 μm diameter pure SiO_2 particles pressed into unreacted pellets of Cu [12], Fe_2O_3 [27,28], or ZnO [27,28] powders.

The X-rays with energies >5 keV are known to have long (>100 μm) penetration range in the SiO_2 solids and materials of comparable density, such as the silicate slags [26,29]. To investigate the significance of the secondary X-ray fluorescence effect in denser materials, such as massicot (PbO), lead ferrite ($Pb_{2+x}Fe_2O_{5+x}$) and magnetoplumbite ($Pb_{1+x}Fe_{12-x}O_{19-x}$), the concentrations of the trace elements (Cu, and Fe) in these phases were remeasured using their corresponding L_α X-rays. The X-rays with low energies (1−2 keV) that could excite the L_α X-rays of Cu (0.93 keV) and Fe (0.705 keV) cannot penetrate far into the sample, and consequently did not result in the secondary fluorescent X-rays from the phase(s) adjacent to that measured, allowing for the solubility of the trace elements to be more accurately measured.

3 Thermodynamic modelling methodologies

The thermodynamic database parameters were optimized using the FactSage 7.3 thermodynamic computer package [30]. The liquid slag and the liquid metal phases were described using the modified quasichemical formalism [31,32], by combining three different types of excess Gibbs free energy parameters: (1) Bragg−Williams, expressed as a polynomial of pure component concentrations, which assumes random mixing configuration entropy; (2) Quasichemical, expressed as a polynomial of the overall composition, which assumes the formation of A−A, A−B, B−B pairs; (3) GUTS, expressed as a polynomial function of the pair fractions. The binary parameters were projected towards the ternary and higher order systems using the geometric formalism developed by CHARTRAND and PELTON [33,34], that combined Kohler (symmetrical), Muggianu (symmetrical) and Toop (asymmetrical) approaches depending on the chemical behavior of the components.

4 Results and discussion

4.1 Experimental results

Backscattered electron micrographs of typical quenched microstructures of the PbO−"$CuO_{0.5}$" (−"$FeO_{1.5}$") samples in equilibrium with metal are shown in Fig. 1. The observed phase assemblages and measured phase compositions of samples in the PbO−"$CuO_{0.5}$" and the PbO−"$CuO_{0.5}$"−"$FeO_{1.5}$" systems are provided in Table S1, and Tables S2−S7 of the Supplementary materials, respectively. The ranges of compositions measured for each solid oxide phase are summarized in Table 1.

The following non-liquid slag phases, in order of increasing brightness on scanning electron micrographs, were identified in the samples:

(1) Spinel ($(Fe,Cu)Fe_2O_4$) – cubic euhedral crystals (taken to be spinel as the EPMA reported that total mass fractions were consistent with mixed Fe^{2+} and Fe^{3+} oxidation state),

(2) Delafossite ($CuFeO_2$) – plate-like euhedral crystals,

(3) Cuprite (Cu_2O) – round anhedral crystals (can appear circular or asymmetrical) (taken to be Cu_2O as the EPMA reported that total mass fractions were consistent with Cu^+ oxidation state),

(4) Cu solid (Cu) – round anhedral particles suspended in liquid slag (can appear circular or asymmetrical),

(5) Magnetoplumbite ($Pb_{1+x}Fe_{12-x}O_{19-x}$) – plate-like euhedral crystals (usually smaller and shorter than delafossite ($CuFeO_2$)),

(6) Copper plumbite (Cu_2PbO_2) – round crystals (may contain entrained copper (Cu) or cuprite (Cu_2O) particles),

(7) Lead ferrite ($Pb_{2+x}Fe_2O_{5+x}$) – subhedral crystals (occasionally comprises of two phases with

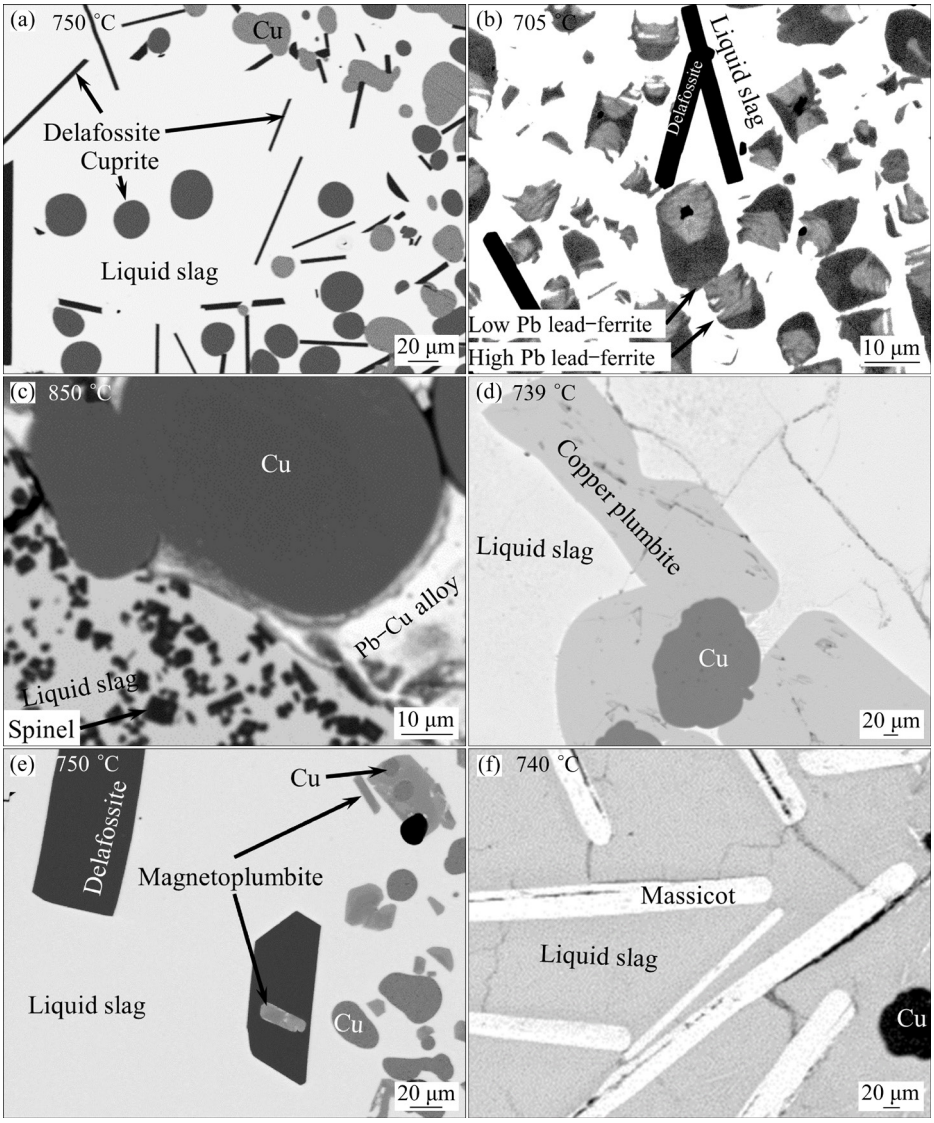

Fig. 1 Backscattered electron micrographs of typical microstructures of PbO−"$CuO_{0.5}$"−("$FeO_{1.5}$") samples in equilibrium with liquid slag and different substances: (a) Cuprite (Cu_2O), delafossite ($CuFeO_2$) and Cu metal; (b) High or low-Pb lead ferrite ($Pb_{2+x}Fe_2O_{5+x}$), delafossite ($CuFeO_2$) and Cu metal (not in frame); (c) Spinel ($(Fe,Cu)Fe_2O_4$), Pb−Cu metal and Cu metal; (d) Copper plumbite (Cu_2PbO_2) and Cu metal; (e) Magnetoplumbite ($Pb_{1+x}Fe_{12-x}O_{19-x}$), delafossite ($CuFeO_2$) and Cu metal; (f) Massicot (PbO) and Cu metal

Table 1 Range of measured compositions of solid oxides (mol.%)

Compound	Formula	PbO		$FeO_{1.5}$		"$CuO_{0.5}$"	
		Min	Max	Min	Max	Min	Max
Massicot	PbO	99.02	100.00		0^{L}	0^{L}	0.03^{L}
Spinel*	$(Fe,Cu)Fe_2O_4$	0.31	0.61	95.18	99.10	0.52	4.31
Cuprite	Cu_2O	0.02	0.06	0.01	0.20	99.74	99.97
Lead−ferrite (high PbO)	$Pb_{2+x}Fe_2O_{5+x}$	54.71	55.13	44.85	55.22		0.02^{L}
Lead−ferrite (low PbO)	$Pb_2Fe_2O_5$	50.69	51.62	48.35	49.30	0.01^{L}	0.03^{L}
Magnetoplumbite	$Pb_{1+x}Fe_{12-x}O_{19-x}$	13.85	16.95	82.76	86.01	0.00^{L}	0.07^{L}
Copper plumbite	Cu_2PbO_2	33.24	33.60	0.00	0.13	66.40	66.73
Delafossite	$CuFeO_2$	0.02	0.10	48.73	50.89	49.08	51.20

* Excluding samples in which crystals were smaller than the minimum probe diameter (~1 μm) and were likely measured inaccurately; ^{L} Concentration of the element was measured using the L_α X-ray instead of the K_α X-ray

two distinct stoichiometries (~50 mol.% and ~54 mol.% PbO, remainder $FeO_{1.5}$) in intimate contact),

(8) Massicot (PbO) – plate-like, round crystals (taken to be massicot as the maximum temperature for the phase transition of litharge (PbO) to massicot was reported to be 600 °C [35]),

(9) Pb−Cu liquid – circular sections of liquid metal suspended in liquid slag (contains SiC crystals (dark, rounded particles introduced during polishing)).

The measured compositions of the non-stoichiometric mixed solid oxides, lead ferrite ($Pb_{2+x}Fe_2O_{5+x}$), magnetoplumbite ($Pb_{1+x}Fe_{12-x}O_{19-x}$) and delafossite ($CuFeO_2$) were analyzed to identify compositional trends and potential solubilities of impurities. Only the composition of the spinel ($(Fe,Cu)Fe_2O_4$) phase was found to depend on the liquid slag composition and the equilibration temperature. Under the conditions of the present study, a maximum concentration of 4.3 mol.% "$CuO_{0.5}$" was measured in the spinel. Two lead ferrite phases were identified: high-PbO ($Pb_9Fe_8O_{21}$) and low-PbO ($Pb_2Fe_2O_5$). All magnetoplumbite ($Pb_{1+x}Fe_{12-x}O_{19-x}$) measured were close in composition to the reduced endmember $Pb_2Fe_{11}O_{18}$ [6]. The delafossite ($CuFeO_2$) phase was measured to be stoichiometric with a 1:1 molar ratio of copper oxide to iron oxide (within the measurement uncertainty of the EPMA) under the conditions of the present study. This observation is consistent with the findings of SCHORNE-PINTO et al [36], who reported that the copper−iron delafossite ($CuFeO_2$) is stoichiometric at 1022 °C and below.

Measurements showed that all solid oxides except spinel ($(Fe,Cu)Fe_2O_4$) do not dissolve significant concentrations of impurities from the present slag system under conditions of the present study. PbO has a maximum solubility of 0.6 mol.% in the spinel ($(Fe,Cu)Fe_2O_4$) phase, consistent with the range of PbO concentration in spinel (Fe_3O_4) reported in a previous study by SHEVCHENKO and JAK [6]. The apparent solubilities of iron and copper impurities in the massicot (PbO), lead ferrite ($Pb_{2+x}Fe_2O_{5+x}$) and magnetoplumbite ($Pb_{1+x}Fe_{12-x}O_{19-x}$) phases were likely overestimated when measured with their K_α X-rays, as measurements made using L_α X-rays consistently showed their solubilities to be close to 0.

4.2 Thermodynamic modelling results and discussion

4.2.1 Liquid slag endmembers and stoichiometric compounds

Thermodynamic model parameters describing litharge (PbO), massicot (PbO), cuprite (Cu_2O), hematite (Fe_2O_3), copper plumbite (Cu_2PbO_2), delafossite ($CuFeO_2$) and the liquid slag endmembers, PbO, and $FeO_{1.5}$, were adopted with modification from previous studies [13,37−39]. The heat capacity of $CuO_{0.5}$ liquid slag end member was revised to better align with calorimetric experimental data by MAH et al [40], while the heat capacity of FeO was revised to better align with the partial molar heat capacity of FeO in the silicate containing slags, as reported by thermodynamic assessments of STEBBINS et al [41], RICHET [42], and LANGE and NAVROTSKY [43]. The heat capacities of the stoichiometric compounds, litharge (PbO), massicot (PbO), cuprite (Cu_2O), hematite (Fe_2O_3) and copper plumbite (Cu_2PbO_2), and all endmembers in the liquid slag were also revised below 25 °C (298.15 K) to better fit low-temperature calorimetric data and to prevent infinite values of heat capacity (and by association, of entropy, enthalpy, and Gibbs free energy) at −273.15 °C (0 K) that may cause errors in some FactSage calculations (e.g., re-stabilization of the liquid slag phase at very low temperatures). The present heat capacities are consistent with the limiting condition necessary to avoid Kauzmann's paradox [44−47]; the calculated entropy of the revised liquid slag endmembers never becomes lower than that of the corresponding solid oxide upon cooling.

The standard enthalpy of formation and entropy of copper plumbite (Cu_2PbO_2) and delafossite ($CuFeO_2$) at 25 °C (298.15 K) were altered to provide a better fit to the experimental data obtained in the present study. The enthalpy of formation of copper plumbite (Cu_2PbO_2) from the elements and its absolute enthalpy at 25 °C (298.15 K) previously reported by CANCAREVIC et al [11] were respectively −413.086 kJ/mol and 135.165 J/(mol·K). The enthalpy of formation was revised to −432.339 kJ/mol to better describe the experimental data of the present study; the discrepancies can arise from (1) contamination of the starting copper plumbite (Cu_2PbO_2) by the quartz (SiO_2) reaction vessel, (2) an excess of lead

oxide in starting mixture used by CANCAREVIC et al [11] (as evidenced by the supplied electron micrographs), (3) the non- equilibrium conditions characteristic of DTA, or (4) reactions between the sample and DTA crucible materials. The enthalpy and entropy of formation of delafossite ($CuFeO_2$) at 25 °C (298.15 K) previously reported by SHISHIN et al [39] were −497.944 kJ/mol and 100.59 J/(mol·K) respectively. These were respectively revised to −494.115 kJ/mol and 103.29 K/(mol·K) to better describe the experimental data of the present study. The entropy of formation was increased by adjusting the heat capacity below −223.15 °C (50 K), including properties describing the antiferromagnetic/ paramagnetic transition of delafossite ($CuFeO_2$). The new peak in heat capacity at the Neel temperature demonstrates reasonable agreement with the range of values reported in literature [48−50]. The enthalpy of formation was adjusted such that the Gibbs free energy of delafossite ($CuFeO_2$) was unchanged at 1145 °C, midway between the previously modelled [18] eutectic temperature corresponding to the reaction:

$$L \rightarrow Cu_2O+CuFeO_2+Cu_{(liquid)}\ (1128\ ^\circ C) \quad (4)$$

And the peritectic temperature corresponding to the reaction:

$$L+Spinel \rightarrow CuFeO_2+Cu_{(liquid)}\ (1162\ ^\circ C) \quad (5)$$

Due to the large uncertainty in solution calorimetry data on the enthalpy of formation of delafossite ($CuFeO_2$) reported by BARANY et al [51], the suitability of the updated parameters was confirmed by comparison of the updated model predictions against studies that reported the $p(O_2)$ over delafossite ($CuFeO_2$) in equilibrium with different phases. $p(O_2)$ vs temperature correlations reported by the studies [52−63] used in the thermodynamic assessment by SHISHIN et al [39] remain well described by the updated parameters.

The new thermodynamic properties of the stoichiometric compounds and liquid slag end-members are presented in Tables S8 and S9 of the Supplementary materials. The properties of stoichiometric compounds, wüstite and liquid slag endmembers are plotted against temperature in Figs. 2−8, with experimental data included for comparison where appropriate.

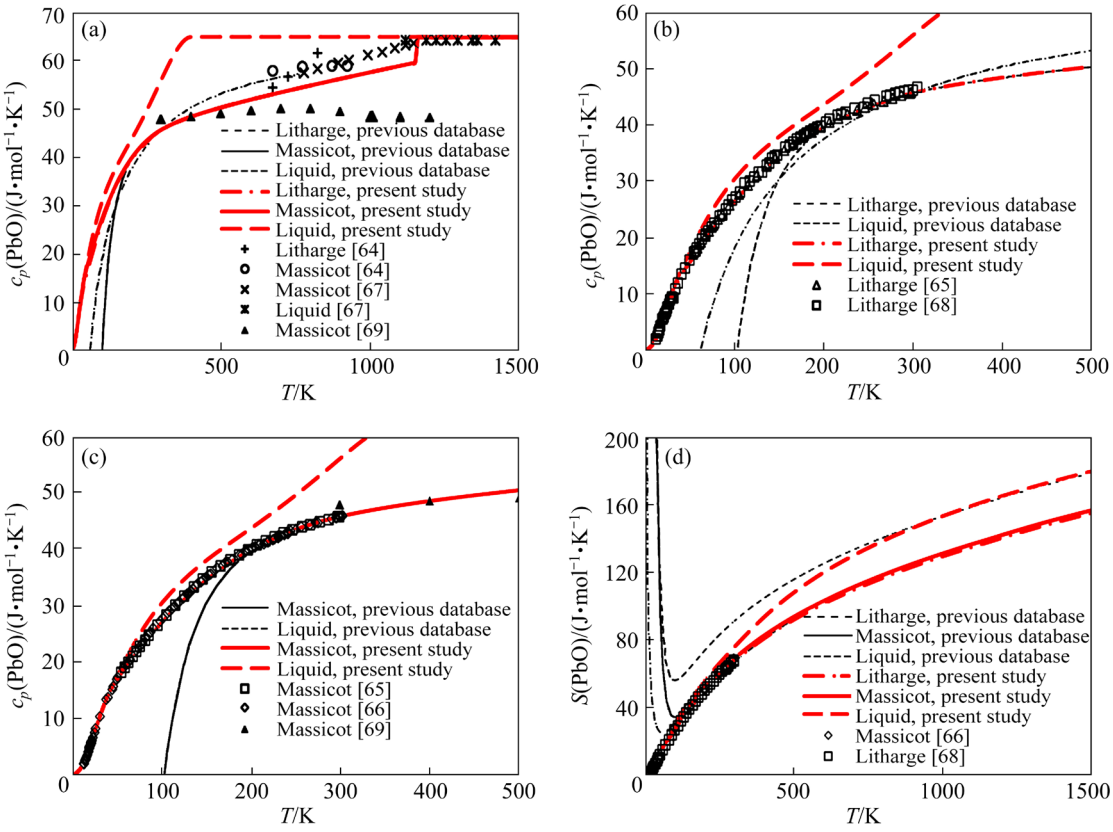

Fig. 2 Heat capacity and entropy of litharge (PbO), massicot (PbO) and (metastable) PbO liquid (Data from the present study, the previous database (parameters optimized by JAK et al [37]), and experimental data from SPENCER and SPICER [64], KING [65], KOSTRYUKOV and MOROZOVA [66], KNACKE and PRESCHER [67], KOSTRYUKOV et al [68] and KOBERTZ [69] are included for comparison)

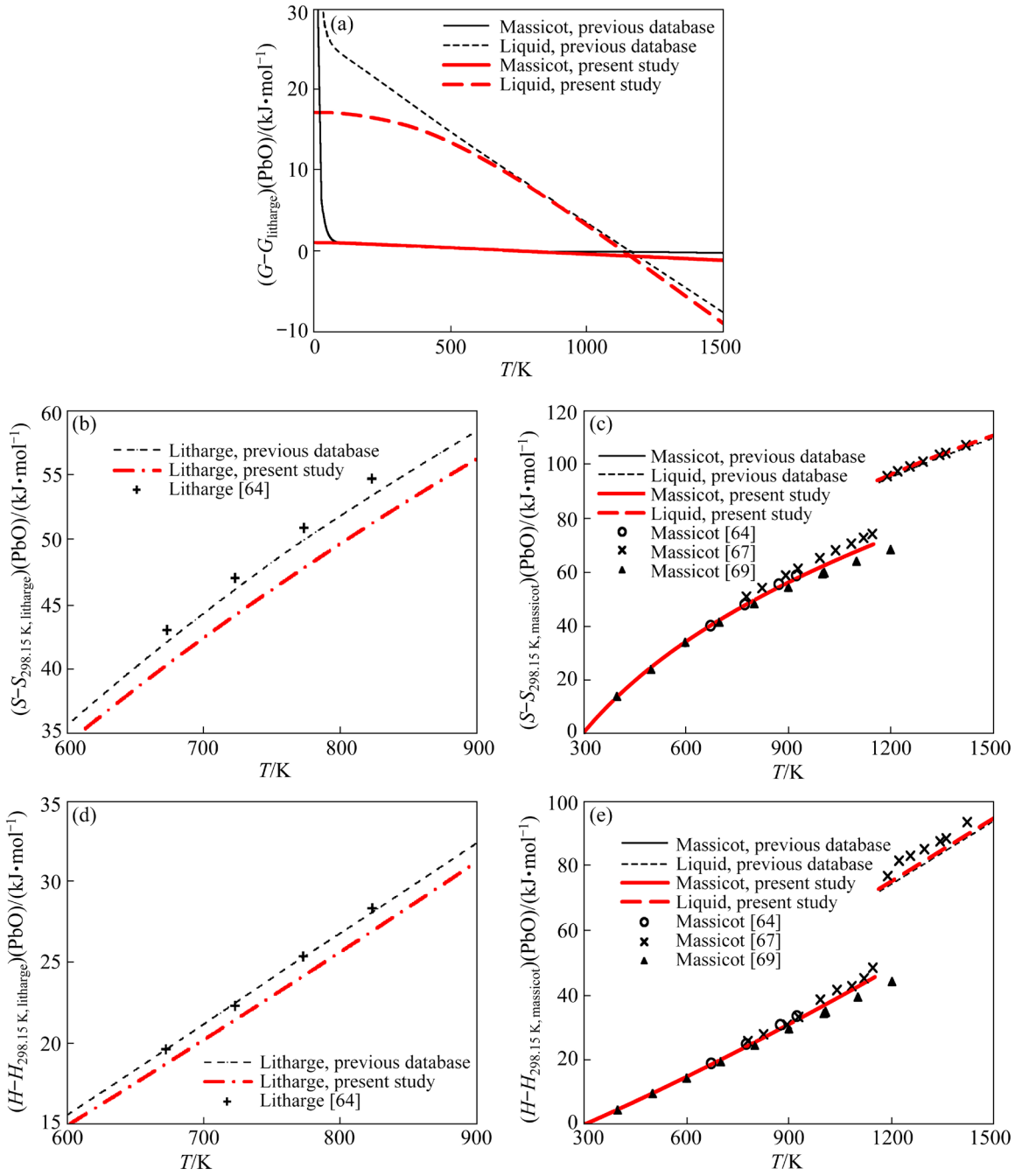

Fig. 3 Gibbs free energy, entropy, and enthalpy differences between litharge (PbO), massicot (PbO) and (metastable) PbO liquid (Data from the present study, the previous database (parameters optimized by JAK et al [37]), and experimental data from SPENCER and SPICER [64], KNACKE and PRESCHER [67], and KOBERTZ [69] are included for comparison)

4.2.2 Solid oxide solution phases

The spinel phase $(Fe^{2+}, Fe^{3+}, Cu^{2+})^{tetr}[Fe^{2+}, Fe^{3+}, Cu^{2+}, Va]^{oct}{}_2O_4^{2-}$, as described using the compound energy formalism with both tetrahedral and octahedral sites, was adopted without modification from HIDAYAT et al [18]. The solubility of PbO was not described in the present thermodynamic model as its maximum solubility in spinel was negligible.

The Bragg−Williams formalisms for lead ferrite ($Pb_2Fe_2O_5$−$Pb_3Fe_2O_6$) and magnetoplumbite ($PbFe_{12}O_{19}$−$Pb_2Fe_{11}O_{18}$) were adopted from SHEVCHENKO and JAK [7] with modifications to the heat capacity of the endmembers below 25 °C

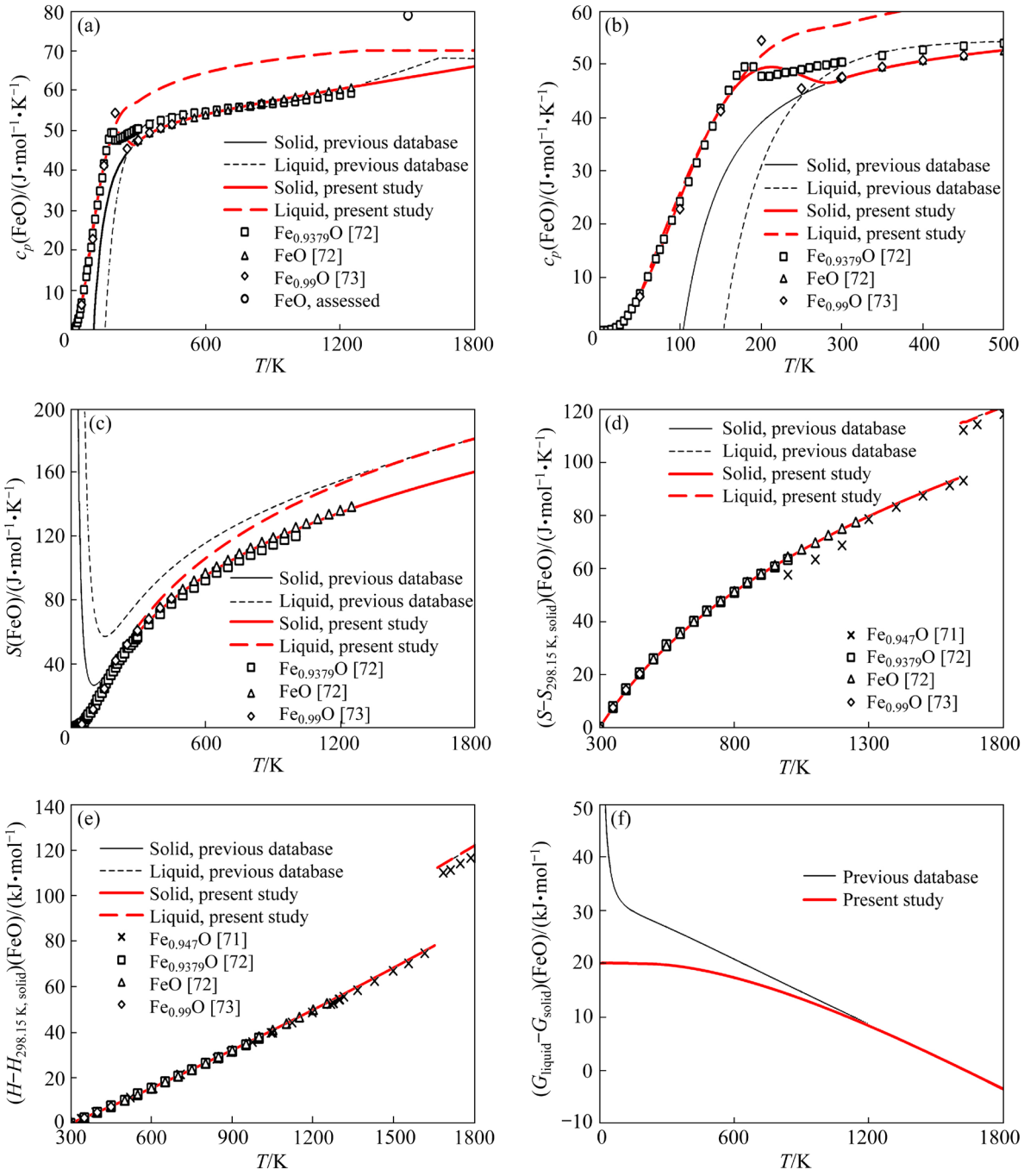

Fig. 4 Heat capacity and entropy of, and entropy, enthalpy and Gibbs free energy differences between FeO endmember in Wüstite and (metastable) FeO liquid (Data from the present study, the previous database (parameters optimized by HIDAYAT et al [70]), experimental data from COUGHLIN et al [71], GRØNVOLD et al [72] and STØLEN et al [73], and the average of the partial molar heat capacities obtained by the thermodynamic assessments of STEBBINS et al [41], RICHET [42], and LANGE and NAVROTSKY [43] are included for comparison; GRØNVOLD et al [72] experimentally measured the heat content of $Fe_{0.9379}O$; Values reported for FeO are based on their modelling of the Wüstite phase)

(298.15 K) to prevent Kauzmann's paradox. The Bragg−Williams formalism for Wüstite (FeO−Fe_2O_3−CuO) was adopted from the works of SHISHIN et al [39] with updates by HIDAYAT et al [70] for the FeO−Fe_2O_3 subsystem, and with modifications to the heat capacity of the FeO endmember below 25 °C (298.15 K) to better fit calorimetric data.

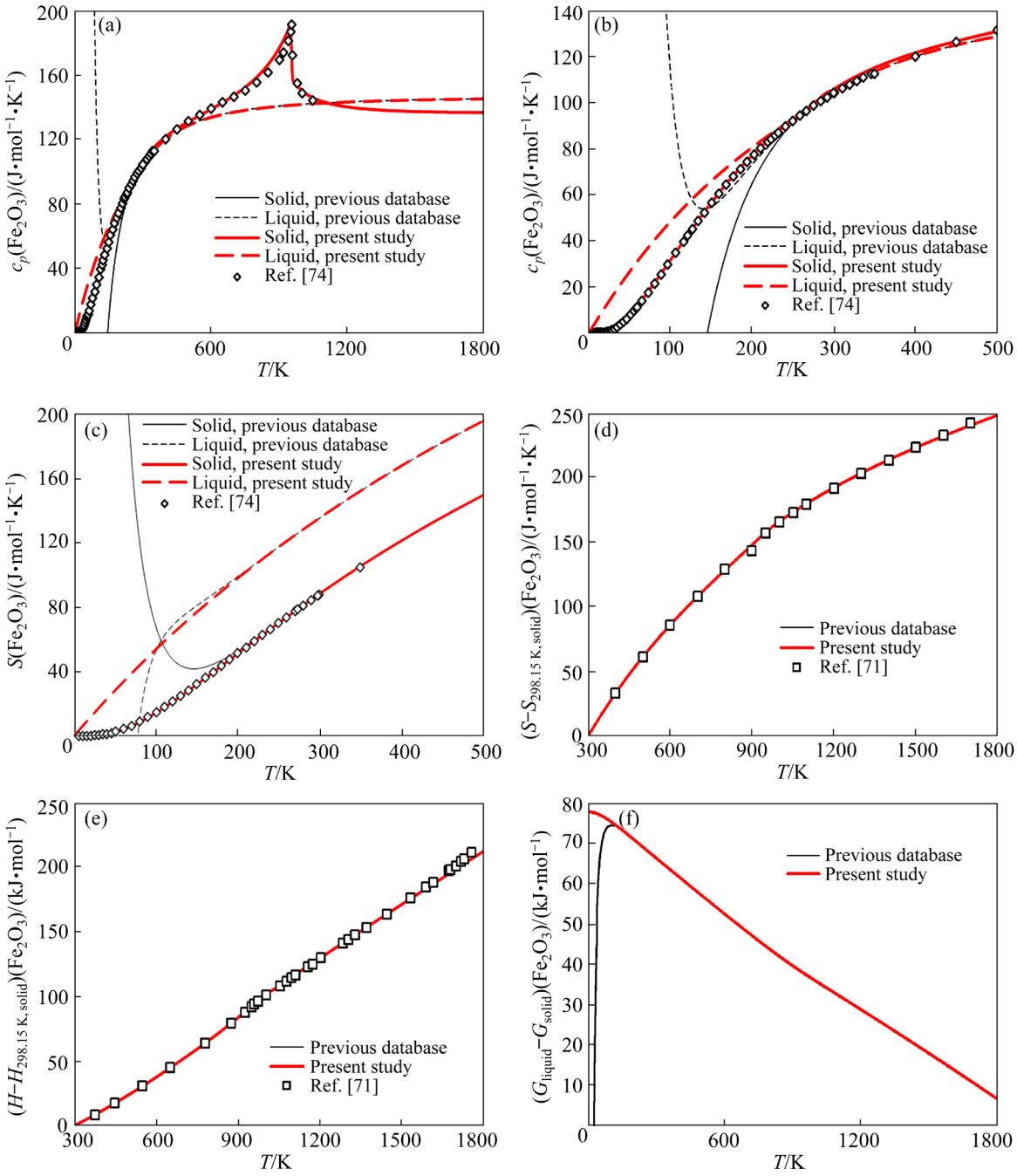

Fig. 5 Heat capacity and entropy of, and entropy, enthalpy, and Gibbs free energy differences between hematite (Fe_2O_3) and (metastable) Fe_2O_3 liquid (Data from the present study, the previous database (parameters optimized by SHISHIN et al [38]), and experimental data from COUGHLIN et al [71], and GRØNVOLD and WESTRUM [74] are included for comparison)

4.2.3 Metallic solution phases (liquid, FCC)

Thermodynamic model parameters describing the liquid metal phase were adopted without modification from SHISHIN and DECTEROV [77] for the Cu−O subsystem, SHISHIN et al [39] for the Cu−Fe−O subsystem, HIDAYAT et al [70] for the Fe−O subsystem, the FSStel and FSCopp FactSage databases for the Fe−Pb and Pb−O systems [30], and HAYES et al [78] for the Pb−Cu system. The binary parameters of the Pb−Cu−Fe liquid system were extrapolated into the ternary system using the Muggianu method, and the binary parameters of the Pb−Cu−O, Pb−Fe−O and Cu−Fe−O systems were extrapolated into the

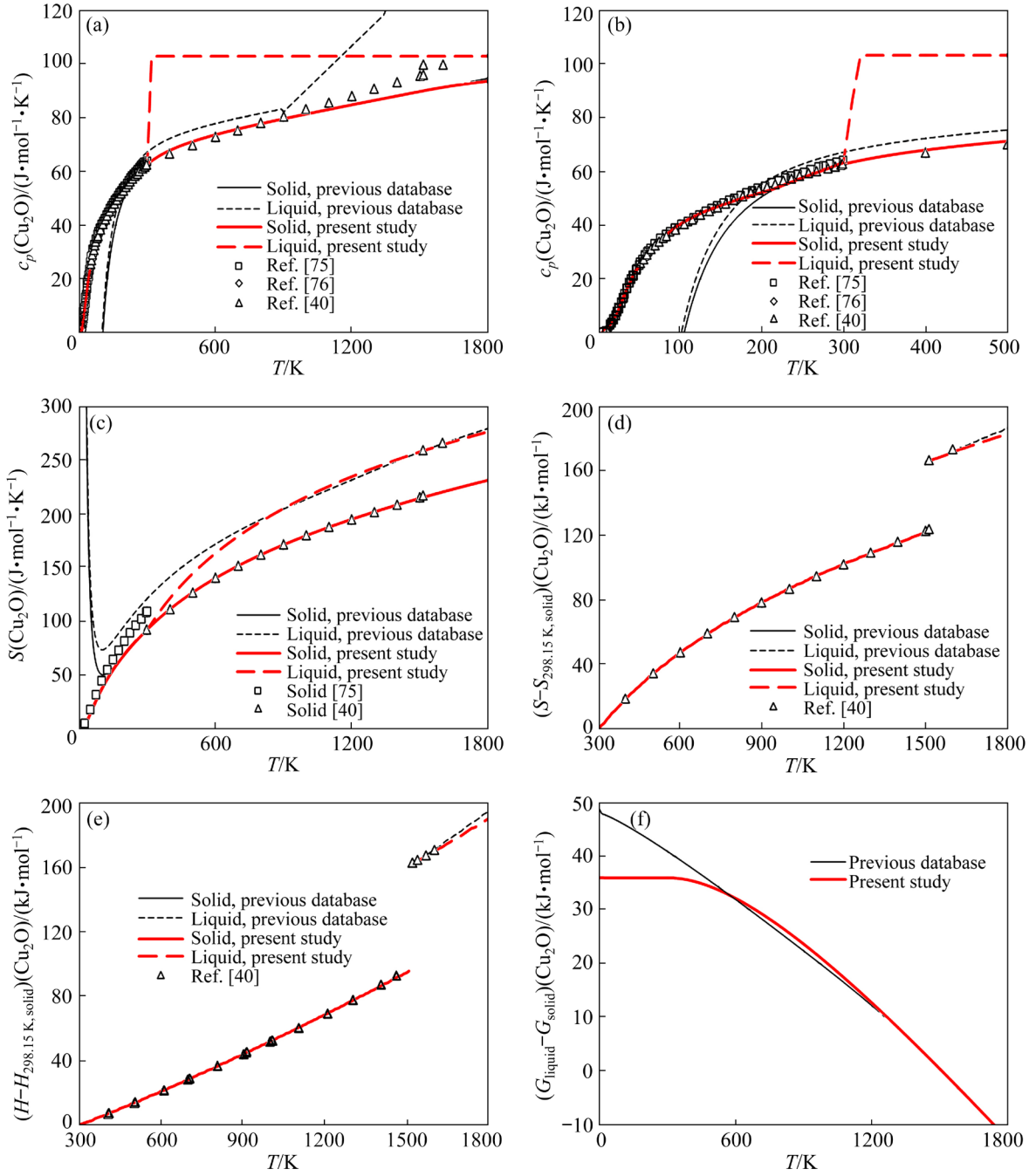

Fig. 6 Heat capacity and entropy of, and entropy, enthalpy and Gibbs free energy differences between cuprite (Cu_2O) and (metastable) Cu_2O liquid (Data from the present study, the previous database (parameters optimized by HIDAYAT et al [18]) and experimental data from HU and JOHNSON [75], GREGOR [76], and MAH et al [40] are included for comparison)

ternary systems using the Kohler/Toop method with oxygen as the asymmetric component. The binary and ternary parameters were extrapolated into the quaternary Pb−Cu−Fe−O system according to the method outlined by CHARTRAND and PELTON [33].

Parameters for the face centered cubic (FCC) solid metal phase, as described using the compound energy formalism, were adopted without the modification from SHISHIN et al [39] for the Cu−O and Cu−Fe subsystems. The parameters describing the Fe−Pb, Pb−O and Pb−Cu subsystems in the FCC phase were adopted from the same studies [30,70,78] as those used to describe the

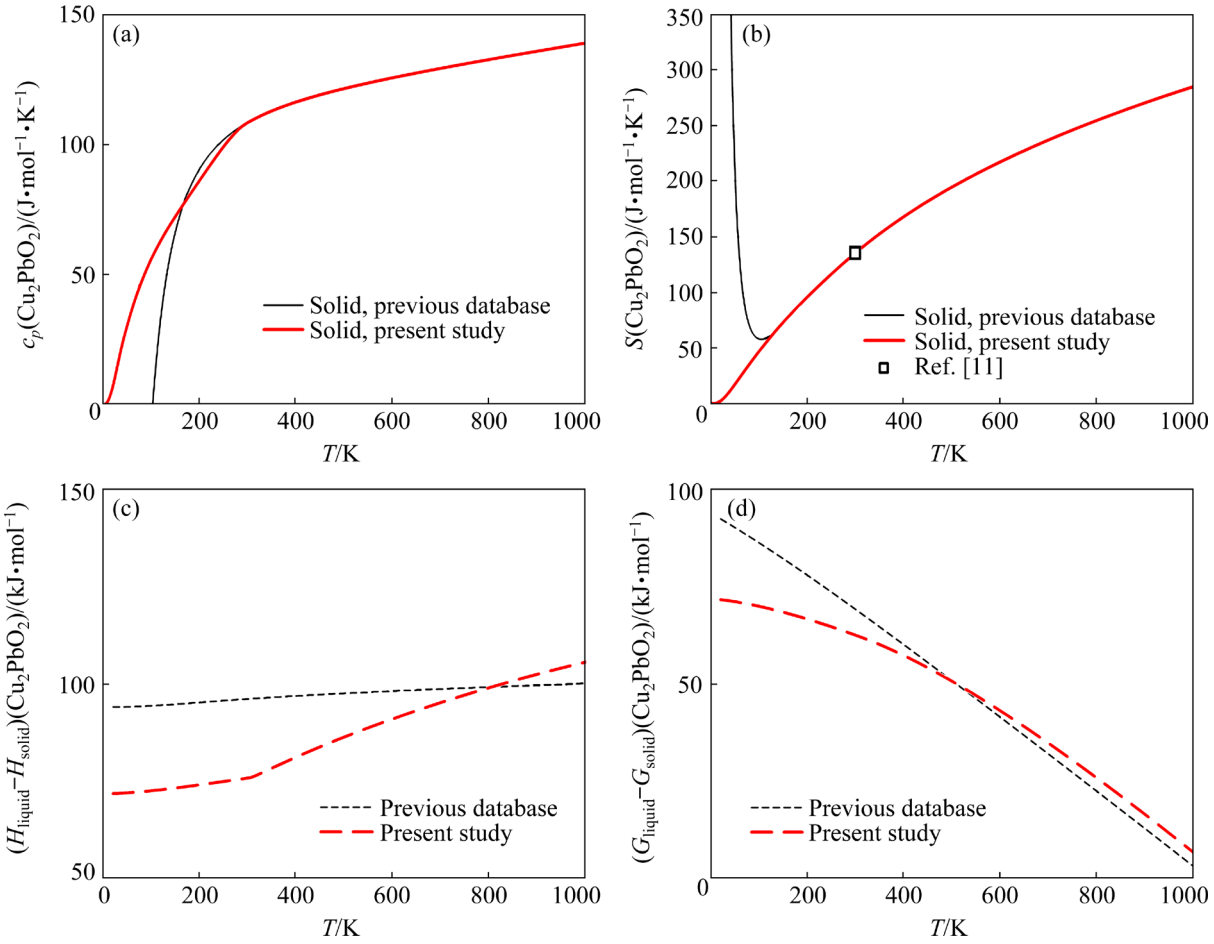

Fig. 7 Heat capacity and entropy of copper plumbite (Cu_2PbO_2), and entropy and Gibbs free energy differences between copper plumbite (Cu_2PbO_2) and (metastable) Cu_2PbO_2 liquid slag (Data from the present study, the previous database (parameters optimized by SHEVCHENKO and JAK [13]) and experimental data from CANCAREVIC et al [11] are included for comparison)

subsystems in the liquid metal phase.

4.2.4 Updated excess properties of liquid slag solution phase

The optimized excess thermodynamic parameters of all solution phases are presented in Table S10 of the Supplementary materials. The binary PbO−"$CuO_{0.5}$" and pseudo-ternary PbO−"$CuO_{0.5}$"−"$FeO_{1.5}$" liquid slag systems were optimized in the present study. Excess parameters for the remaining systems were adopted without modification from studies by HIDAYAT et al [18,79] for the FeO−$FeO_{1.5}$ binary system and the "$CuO_{0.5}$"−FeO−$FeO_{1.5}$ ternary system, and from SHEVCHENKO and JAK [7] for the PbO−FeO−$FeO_{1.5}$ ternary slag system. The Kohler method was used to extrapolate binary parameters into all ternary systems except of the "$CuO_{0.5}$"−FeO−$FeO_{1.5}$ ternary system, which used Kohler/Toop grouping with $CuO_{0.5}$ as asymmetrical component. The binary and ternary parameters were extrapolated into the quaternary PbO−$CuO_{0.5}$−FeO−$FeO_{1.5}$ system according to the method outlined by CHARTRAND and PELTON [33].

The excess Gibbs free energy of the binary PbO−"$CuO_{0.5}$" and ternary PbO−"$CuO_{0.5}$"−"$FeO_{1.5}$" liquid slag systems were optimized to minimize the root mean square (RMS) deviation of calculated liquidus temperature from the experimental data. The temperature root mean error of entire system and individual primary phase fields was calculated as

$$\mathrm{RMS}_{\mathrm{error,T}}=\sqrt{\frac{\Sigma\left(T_{\mathrm{calc}}-T_{\mathrm{exp}}\right)^2}{N}}=\sqrt{\frac{\Sigma\Delta T^2}{N}} \tag{6}$$

where N is the number of experiments, and T represents calculated or experimentally determined the slag liquidus temperature. For comparison, the

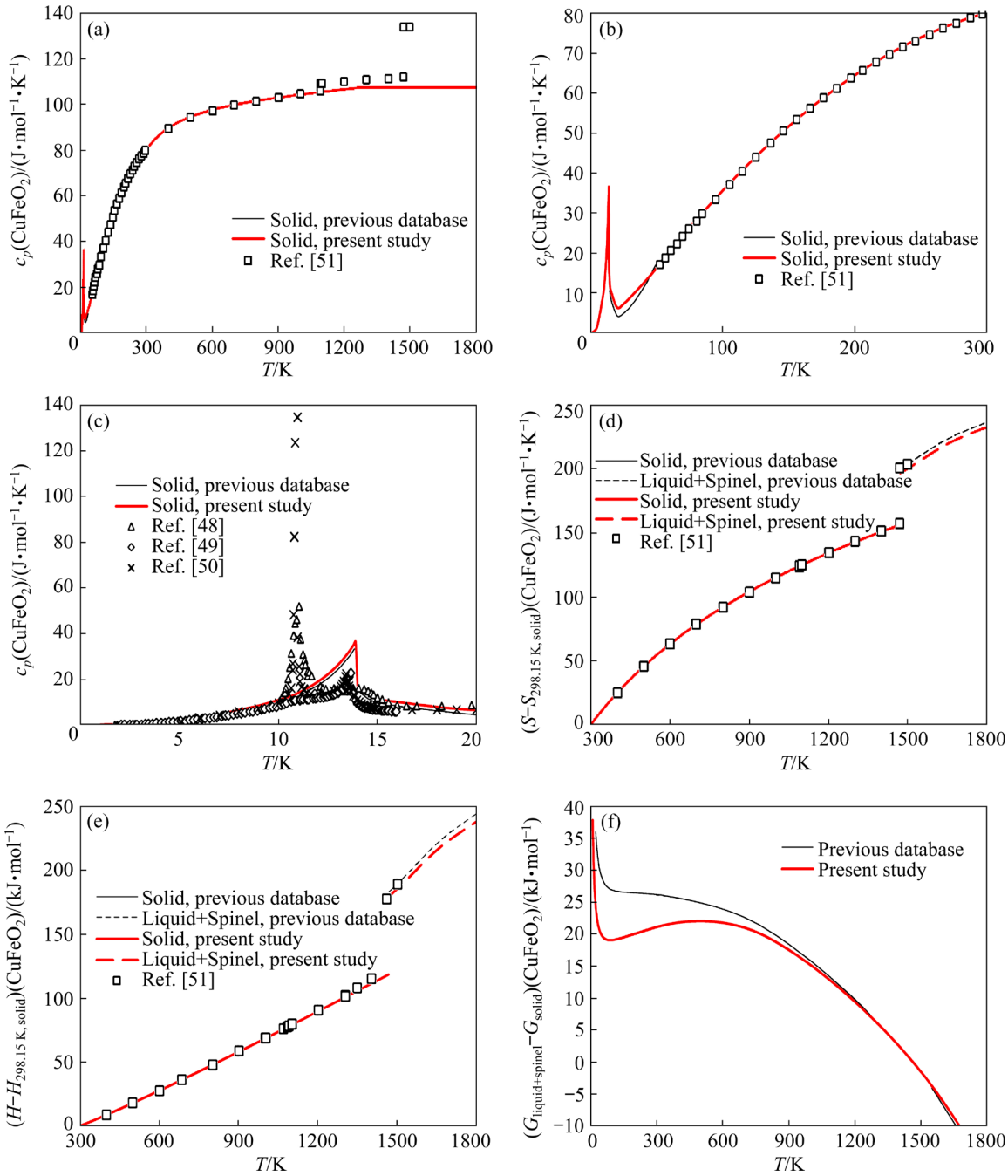

Fig. 8 Heat capacity and entropy of delafossite ($CuFeO_2$), and entropy, enthalpy and Gibbs free energy differences between delafossite ($CuFeO_2$) and (metastable) liquid slag + spinel ($(Fe,Cu)Fe_2O_4$) mixture with bulk composition $CuFeO_2$ (Data from the present study, the previous database (parameters optimized by SHISHIN et al. [39]) and experimental data from BARANY et al [51], TAKEDA et al [48], MITSUDA et al [49] and PETRENKO et al [50] are included for comparison; Note: the entropy of delafossite ($CuFeO_2$) reported by BARANY et al [51] was not considered in the optimization as they did not account for the antiferromagnetic/paramagnetic transition in delafossite at 10−15 K)

compositional root mean square error was also calculated by using the liquid slag composition error in place of temperature error, where the compositional error of each point was calculated as

$$\Delta X = \sqrt{[\Sigma(X_{i,\text{calculated}} - X_{i,\text{experimental}})^2]/4} \quad (7)$$

The temperature and compositional RMS values of the PbO−"$CuO_{0.5}$" pseudo-binary and the PbO−"$CuO_{0.5}$"−"$FeO_{1.5}$" pseudo-ternary systems are presented in Table 2 (with comparison to the RMS errors of the model by SHEVCHENKO and JAK [13]) and Table 3, respectively.

Although properties of delafossite ($CuFeO_2$) and the $CuO_{0.5}$ and FeO slag endmembers were altered above 298 K in the present study, the experimental studies [14,16,17] that were weighted the most heavily in the assessment of the "$CuO_{0.5}$"−FeO−$FeO_{1.5}$ ternary system by HIDAYAT et al [18] remained described when performing calculations using the previously obtained excess parameters with the new $CuO_{0.5}$ endmember; this is demonstrated by the calculated invariant points remaining unchanged (shown in Table 4). Likewise, the modification of the FeO liquid slag endmember did not result in significant changes to the thermodynamic description of PbO−FeO−$FeO_{1.5}$ system from previous thermodynamic assessment by SHEVCHENKO and JAK [7].

Table 2 Comparisons of RMS error values of modelled PbO−"$CuO_{0.5}$" system in equilibrium with metal, as calculated using parameters by SHEVCHENKO and JAK [13] and re-optimized database produced in present study

Phase	Number of points	Present work						SHEVCHENKO and JAK [13]					
		ΔT			$\Delta X_{\text{liquid slag}}$			ΔT			$\Delta X_{\text{liquid slag}}$		
		Min	Max	RMS	Min	Max	RMS	Min	Max	RMS	Min	Max	RMS
Cuprite (Cu_2O)	9*	−7.25	2.71	3.91	0.08	0.72	0.39	−22.06	25.95	14.44	0.34	3.23	1.81
Copper plumbite (Cu_2PbO_2)	3	−0.20	3.30	1.96	0.07	1.04	0.62	−24.10	−21.52	22.57	9.49	10.09	9.80
Massicot (PbO)	4	−5.44	4.99	4.11	0.49	1.23	0.92	−10.94	0.28	7.04	0.06	2.58	1.66
Total	16	−7.25	4.99	3.68	0.07	1.23	0.61	−24.10	25.95	15.01	0.06	10.09	4.53

* Includes points from 880 to 920 °C from the previous study of PbO−"$CuO_{0.5}$" system by SHEVCHENKO and JAK [12]

Table 3 RMS error values of modelled PbO−"$CuO_{0.5}$"−"$FeO_{1.5}$" system in equilibrium with metal, as calculated using re-optimized database produced in present study

Phase	Number of points	ΔT			$\Delta X_{\text{liquid slag}}$		
		Min	Max	RMS	Min	Max	RMS
Massicot (PbO)	16	−12.77	16.56	10.61	0.06	2.95	1.82
Spinel ($(Fe,Cu)Fe_2O_4$)	6	−25.44	65.00	29.90	0.15	2.17	1.14
Cuprite (Cu_2O)	17*	−15.12	11.51	7.18	0.08	1.87	0.78
Lead ferrite ($Pb_{2+x}Fe_2O_{5+x}$)	3	14.66	26.25	21.31	4.85	9.66	7.38
Magnetoplumbite ($Pb_{1+x}Fe_{12-x}O_{19-x}$)	15	−4.34	50.18	20.88	0.02	5.02	1.94
Copper plumbite (Cu_2PbO_2)	15	−11.64	8.98	5.44	0.07	3.39	1.73
Delafossite ($CuFeO_2$)	22	−27.05	31.68	16.14	0.10	4.16	2.12
Total	94*	−27.05	65.00	15.21	0.02	9.66	2.13

* Includes points from 880 to 920 °C from the previous study of PbO−"$CuO_{0.5}$" system by SHEVCHENKO and JAK [12]

Table 4 Comparison of invariant points in "$CuO_{0.5}$"−"FeO_x" binary subsystem in equilibrium with metallic copper, as calculated using parameters by HIDAYAT et al [18] and re-optimized database produced in present study

Temperature/°C		Reaction	"FeO_x" content in slag/mol.%	
Previous model	Present study		HIDAYAT et al [18]	Present study
1128	1129	L→Cuprite (Cu_2O)+Delafossite ($CuFeO_2$)+$Cu_{(liquid)}$	18.1	18.2
1162	1163	L+Spinel ($(Fe,Cu)Fe_2O_4$)→ Delafossite($CuFeO_2$)+$Cu_{(liquid)}$	25.5	25.5
1397	1398	L→Spinel($(Fe,Cu)Fe_2O_4$)+Wüstite+$Cu_{(liquid)}$	94.6	94.6

4.3 Comparison of thermodynamic modelling outcomes with experimental data

The calculated phase diagrams of the PbO−"$CuO_{0.5}$"−"$FeO_{1.5}$" pseudo-binary and the PbO−"$CuO_{0.5}$"−"$FeO_{1.5}$" pseudo-ternary systems are given in Figs. 9 and 10, respectively. A detailed inset of the PbO−"$CuO_{0.5}$"−"$FeO_{1.5}$" pseudo-ternary phase diagram is given in Fig. 11. The PbO−"$CuO_{0.5}$"−"$FeO_{1.5}$" pseudo-ternary phase diagram and its inset without experimental points overlaid are given in Figs. S1 and S2 of the Supplementary materials, respectively. A plot of "$CuO_{0.5}$" content in spinel ($(Fe,Cu)Fe_2O_4$) against the "$CuO_{0.5}$" content in the liquid slag at different isotherms is shown in Fig. 12.

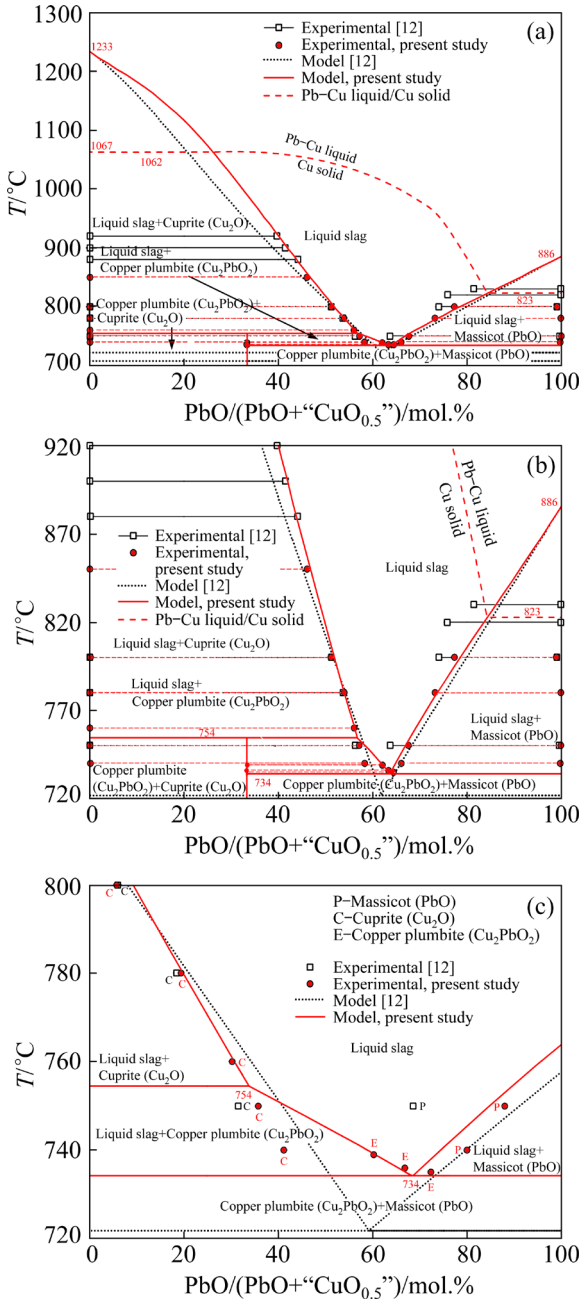

Fig. 9 Phase diagrams of PbO−"$CuO_{0.5}$" pseudo-binary system in equilibrium with metal, calculated using optimized thermodynamic parameters obtained in present study (For comparison, the phase diagram previously published by SHEVCHENKO and JAK [13], and experimental data from the present study and from SHEVCHENKO and JAK [12] are included)

The modelled PbO−"$CuO_{0.5}$" pseudo-binary phase diagram contains three primary phase fields: massicot (PbO, melting point 886 °C), cuprite (Cu_2O, melting point 1233 °C) and copper plumbite (Cu_2PbO_2), with a eutectic point between copper plumbite (Cu_2PbO_2) and massicot (PbO) at 63.7 mol.% PbO in liquid slag and 734 °C. The copper plumbite (Cu_2PbO_2) phase melts incongruently at 754 °C forming cuprite (Cu_2O), and liquid slag containing 56.9 mol.% PbO. Additionally, the projection of the copper rich Cu−Pb solid alloy/Pb−Cu liquid alloy phase boundary onto the phase diagram is included for reference, showing that the melting point of the copper-rich alloy decreases with increasing PbO concentration in the slag. The list of invariant reactions of the PbO−"$CuO_{0.5}$" pseudo-binary system in equilibrium with copper rich solid alloy and (Pb−)Cu liquid, along with the modelled liquid slag, solid and liquid alloys compositions, is presented in Table 5. Upon melting, the Pb concentration of the metallic phase increases significantly due to the reduction of PbO in the slag by metallic copper.

In the PbO−"$CuO_{0.5}$" pseudo-binary system, several discrepancies between the experimental data from the present study and previous studies were identified. Preliminary experiments demonstrated that the incongruent melting/recrystallisation of copper plumbite (Cu_2PbO_2) to/from the liquid slag and cuprite (Cu_2O) through the reaction $Cu_2PbO_{2(solid)} \rightleftharpoons Slag_{(liquid)} + Cu_2O_{(solid)}$ was kinetically inhibited, and that metastable copper plumbite (Cu_2PbO_2) may even be found in samples of the massicot (PbO) primary phase field equilibrated at up to 40 °C above the binary eutectic temperature. To accurately characterize the primary phase fields of the PbO−"$CuO_{0.5}$" system between 730 and 750 °C, the equilibrium condition was approached from two different directions; in one set of experiments all samples were preheated to 800 °C prior to equilibration (yielding cuprite (Cu_2O) and

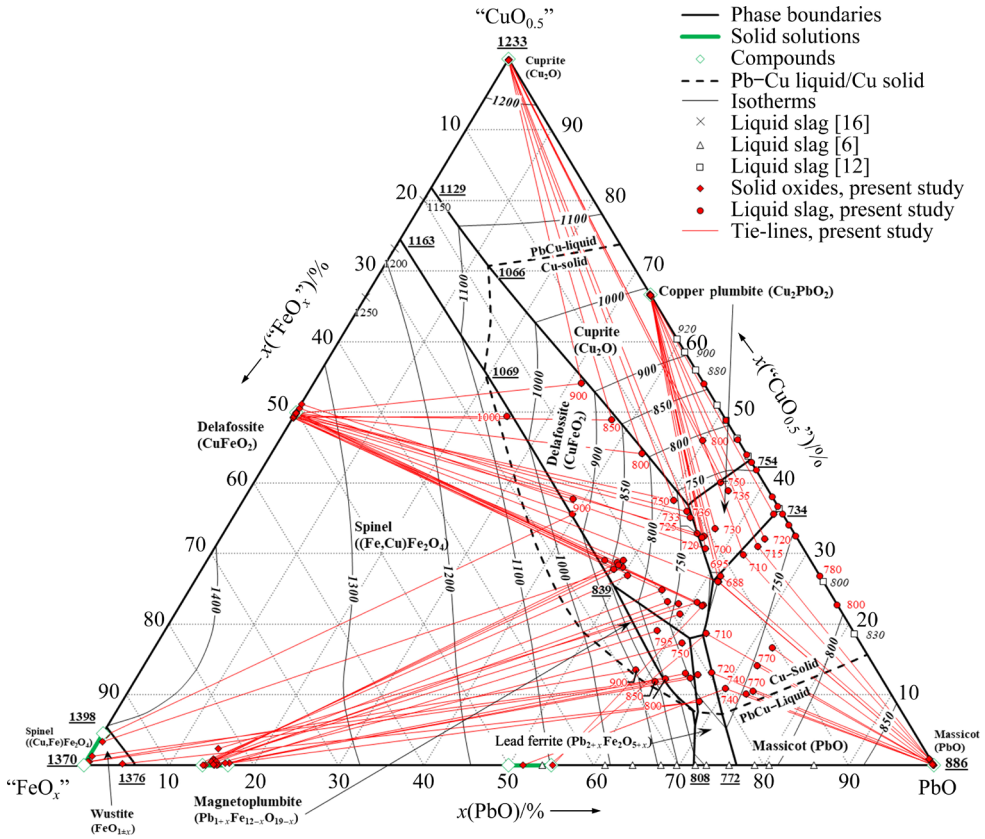

Fig. 10 Liquidus surface of PbO−"$CuO_{0.5}$"−"$FeO_{1.5}$" pseudo-ternary system in equilibrium with metal (Phase boundaries and isotherms were calculated using the database developed in the present study, while solid solution compositional ranges are based on experimental data; Experimental data from the present study and from previous studies [6,12,16] are included for comparison)

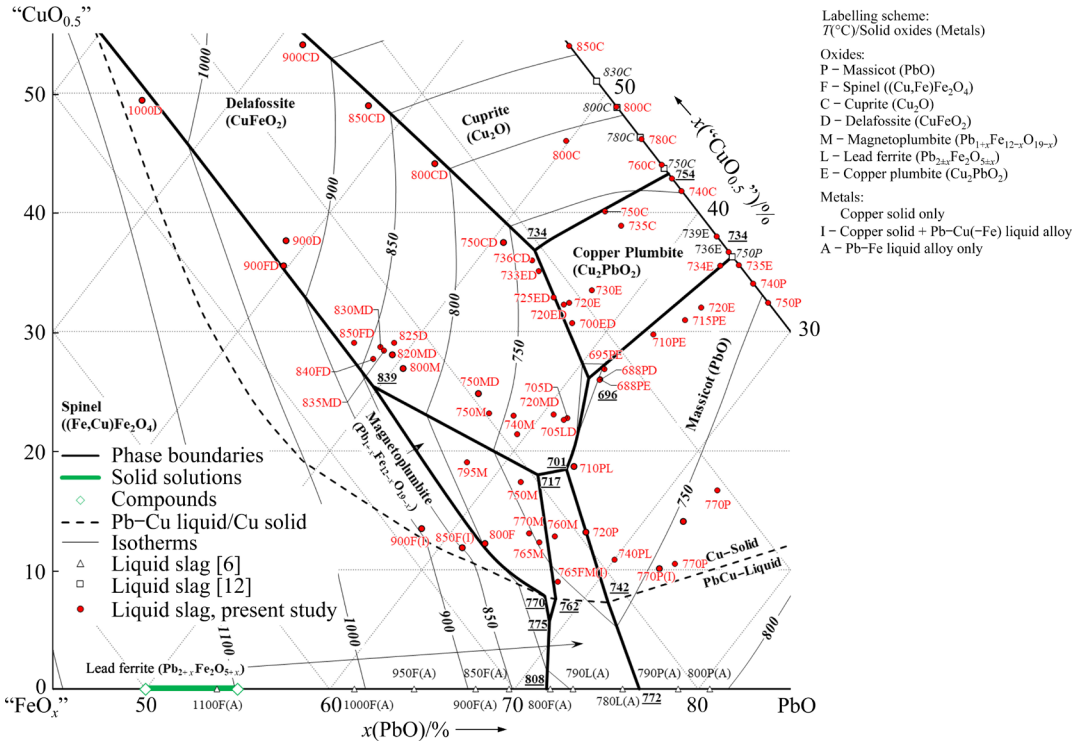

Fig. 11 Detail of PbO−"$CuO_{0.5}$"−"$FeO_{1.5}$" pseudo-ternary phase diagram in equilibrium with metal (Experimental data from the present study and from previous studies [6,12] are included for comparison)

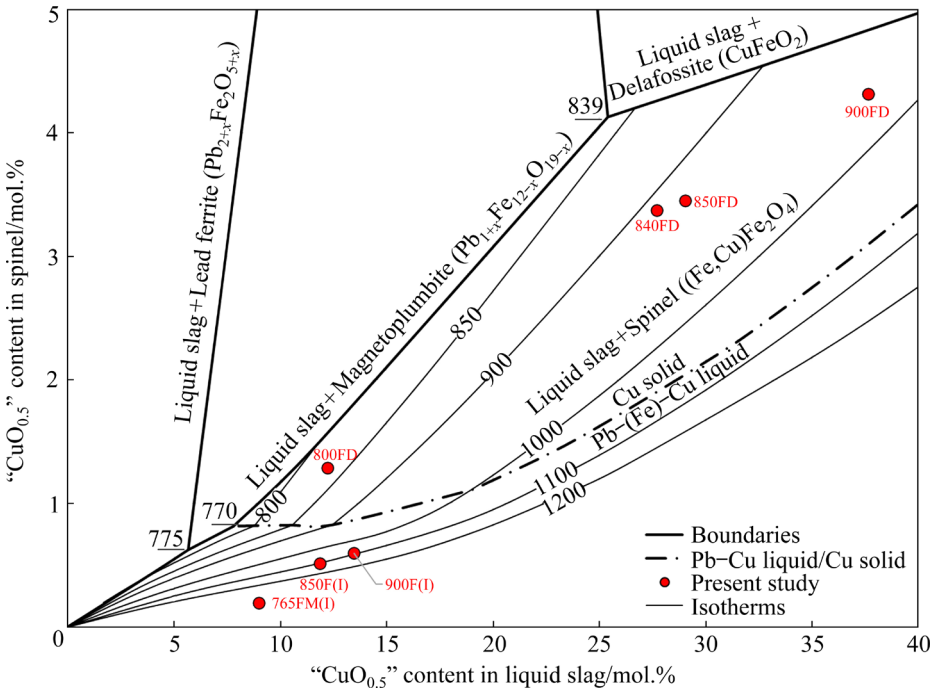

Fig. 12 Composition of spinel ($(Fe,Cu)Fe_2O_4$) in equilibrium with PbO−"$CuO_{0.5}$"−"$FeO_{1.5}$" liquid slag

Table 5 Invariants points of PbO−"$CuO_{0.5}$" pseudo-ternary system in equilibrium with copper-rich Cu(−Pb) solid alloy and (Pb−)Cu liquid, as calculated using optimized thermodynamic model

Temperature/ °C	Reaction	Phase	Type	Composition/mol.%		
				Pb	Cu	O
1067	L_{Cu}→Cuprite (Cu_2O)+Cu_{solid}	L_{Cu}	M		99.57	0.43
		Cu_{solid}	M		99.98	0.02
1062	L_{PbCu}→L_{slag}+Cuprite (Cu_2O)+Cu_{solid}	L_{slag}	O	26.2	73.8	
		L_{PbCu}	M	0.52	97.7	1.77
		Cu_{solid}	M	0.05	99.93	0.02
823	L_{slag}+L_{PbCu}→Massicot (PbO)+Cu_{solid}	L_{slag}	O	84.3	15.7	
		L_{PbCu}	M	87.6	11.8	0.56
		Cu_{solid}	M	0.35	99.65	0.00

Oxide phases are designated "O" while metallic phases are designated "M"; Product side represent products formed on cooling

liquid slag), while in another set all samples were preheated to 20 °C above the final equilibration temperature prior to equilibration (yielding copper plumbite (Cu_2PbO_2) and liquid slag). The liquid slag compositions from these experiments were used to construct the cuprite (Cu_2O) and copper plumbite (Cu_2PbO_2) primary phase fields in the thermodynamic modelling. The finding that the copper plumbite (Cu_2PbO_2) melted incongruently contradicted the results of previous studies [8,10,11] except of HOFFMANN and KOHLMEYER [9] and SHEVCHENKO and JAK [12]. In the massicot (PbO) and cuprite (Cu_2O) primary phase fields, the differences in the liquidus temperatures and compositions of the liquid slags between the present study and studies [8−11] predating that of SHEVCHENKO and JAK [12] were attributed to a combination of cross- contamination of the liquid slag by crucible materials, kinetic factors inhibiting the decomposition/recrystallisation of the copper plumbite (Cu_2PbO_2) phase and the delayed response of thermal analysis techniques to phase changes. The present study agrees well with the findings of SHEVCHENKO and JAK [12] in the cuprite (Cu_2O)

primary phase field, but less well in the massicot (PbO) primary phase field; this was attributed to the improved quenching of the liquid slag in the present study.

In the PbO−"$CuO_{0.5}$"−"$FeO_{1.5}$" pseudo-ternary system, the liquidus temperatures and phase compositions for slags in the massicot (PbO), spinel ($(Fe,Cu)Fe_2O_4$), cuprite (Cu_2O), lead ferrite ($Pb_{2+x}Fe_2O_{5+x}$), magnetoplumbite ($Pb_{1+x}Fe_{12-x}O_{19-x}$), copper plumbite ($Cu_2PbO_2$), and delafossite ($CuFeO_2$) primary phase fields were experimentally determined between 688 and 1000 °C for the first time. The modelled PbO−"$CuO_{0.5}$"−"$FeO_{1.5}$" pseudo-ternary phase diagram contains eight primary phase fields: massicot (PbO, melting point 886 °C), spinel ($(Fe,Cu)Fe_2O_4$)), Wüstite (FeO, melting point 137 °C) cuprite (Cu_2O, melting point 1233 °C), lead ferrite ($Pb_{2+x}Fe_2O_{5+x}$), magnetoplumbite ($Pb_{1+x}Fe_{12-x}O_{19-x}$), copper plumbite ($Cu_2PbO_2$), and delafossite ($CuFeO_2$). The liquid slag and liquid Pb−Cu alloy compositions at the invariant points (11 total) predicted by the thermodynamic model obtained in the present study are summarized in Table 6. The two modifications of lead−ferrite ($Pb_{2+x}Fe_2O_{5+x}$) were described using a single primary phase field, as there is limited experimental data on which the lead−ferrite phase is stable at a given condition.

Table 6 Invariants points of PbO−"$CuO_{0.5}$"−"$FeO_{1.5}$" pseudo-ternary system, as calculated using optimized thermodynamic model

Reaction type	Temperature/ °C	Reaction	Phase	Phase type	Composition/mol.%			
					Pb	Cu	Fe	O
Liquid slag in equilibrium with three solid oxides and one metal	696	L_{slag}→Massicot (PbO)+Copper plumbite (Cu_2PbO_2)+Delafossite ($CuFeO_2$)+Cu_{solid}	L_{slag}	O	61.0	26.1	12.9	
	701	L_{slag}→Massicot (PbO)+Lead ferrite+ Delafossite ($CuFeO_2$)+Cu_{solid}	L_{slag}	O	63.6	18.4	17.9	
	717	L_{slag}+Magnetoplumbite ($Pb_{1+x}Fe_{12-x}O_{19-x}$→ Lead ferrite ($Pb_{2+x}Fe_2O_{5+x}$)+ Delafossite ($CuFeO_2$)+$Cu_{solid}$	L_{slag}	O	62.3	18.0	19.7	
	734	L_{slag}+Cuprite (Cu_2O)→ Copper plumbite (Cu_2PbO_2)+ Delafossite ($CuFeO_2$)+Cu_{solid}	L_{slag}	O	52.7	36.8	10.5	
	775	L_{slag}+Magnetoplumbite ($Pb_{1+x}Fe_{12-x}O_{19-x}$)+→ Spinel ($(Fe,Cu)Fe_2O_4$)+ Lead ferrite ($Pb_{2+x}Fe_2O_{5+x}$) +$L_{PbCu}$	L_{slag}	O	69.1	5.7	25.3	
			L_{PbCu}	M	94.4	5.3	0.00	0.28
	839	L_{slag}+Spinel ($(Fe,Cu)Fe_2O_4$)→ Magnetoplumbite ($Pb_{1+x}Fe_{12-x}O_{19-x}$)+ Delafossite ($CuFeO_2$)+$Cu_{solid}$	L_{slag}	O	49.6	25.4	25.0	
Liquid slag in equilibrium with two solid oxides and two metals	742	L_{slag}+L_{PbCu}→Massicot (PbO)+ Lead ferrite ($Pb_{2+x}Fe_2O_{5+x}$)+Cu_{solid}	L_{slag}	O	71.4	7.3	21.3	
			L_{PbCu}	M	92.9	6.9	0.00	0.22
	762	L_{slag}+Magnetoplumbite ($Pb_{1+x}Fe_{12-x}O_{19-x}$)+ L_{PbCu}→Lead ferrite ($Pb_{2+x}Fe_2O_{5+x}$)+Cu_{solid}	L_{slag}	O	68.5	7.6	24.0	
			L_{PbCu}	M	91.9	7.9	0.00	0.26
	770	L_{slag}+Spinel ($(Fe,Cu)Fe_2O_4$)→ Magnetoplumbite ($Pb_{1+x}Fe_{12-x}O_{19-x}$)+ L_{PbCu}+Cu_{solid}	L_{slag}	O	67.8	7.8	24.4	
			L_{PbCu}	M	91.4	8.3	0.00	0.27
	1066	Delafossite ($CuFeO_2$)+L_{PbCu}→ L_{slag}+Cuprite (Cu_2O)+Cu_{solid}	L_{slag}	O	12.2	70.8	17.1	
			L_{PbCu}	M	0.41	98.5	0.00	1.1
	1069	Spinel ($(Fe,Cu)Fe_2O_4$)+L_{PbCu}→ L_{slag}+Delafossite ($CuFeO_2$)+Cu_{solid}	L_{slag}	O	19.2	55.9	24.9	
			L_{PbCu}	M	0.17	98.1	0.00	1.7

Oxide phases are designated "O" while metallic phases are designated "M"; Product side represent products formed on cooling

5 Conclusions

(1) The phase equilibria of the PbO−"$CuO_{0.5}$" and PbO−"$CuO_{0.5}$"−"$FeO_{1.5}$" slag systems in equilibrium with solid metallic copper and/or liquid metallic lead−copper alloy were experimentally investigated between 688 and 1000 °C.

(2) In the PbO−"$CuO_{0.5}$" pseudo-binary system, the present study resolved the uncertainty on the stable phase assemblages near the eutectic temperature; the copper plumbite (Cu_2PbO_2) phase was found modelled to melt incongruently in the PbO−"$CuO_{0.5}$" subsystem to form cuprite (Cu_2O) and the liquid slag, in contrast to previous studies that suggested it apparently decomposed peritectoidally below binary eutectic temperature to form massicot (PbO) and cuprite (Cu_2O).

(3) Experimental data were obtained for the PbO−"$CuO_{0.5}$"−"$FeO_{1.5}$" pseudo-ternary slag system for the first time. A self-consistent thermodynamic database was developed to explain the new experimental data, in which fundamental improvements were made to the thermodynamic descriptions of the stoichiometric compounds and the end members of several solution phases (liquid slag, lead ferrite ($Pb_2Fe_2O_5$−$Pb_3Fe_2O_6$), magnetoplumbite ($PbFe_{12}O_{19}$−$Pb_2Fe_{11}O_{18}$), and Wüstite (FeO−Fe_2O_3−CuO)).

(4) The revised model more accurately described liquid slag heat capacities in the range of temperatures relevant to pyrometallurgical processes, and partially eliminated infinite values of heat capacity, enthalpy, entropy and Gibbs free energy at 0 K. This study forms part of a broader study of the 19-element multicomponent system for nonferrous metal smelting and recycling industries.

Acknowledgments

The authors would like to thank research assistants (Ms. Suping HUANG, Mrs. Marina CHERNISHOVA, Ms. Samaneh ASHJAA, Mr. Ryan WRIGHT) at the Pyrometallurgy Innovation Centre and the staff of the Centre for Microscopy and Microanalysis (CMM) for their technical expertise and assistance in producing the research outcomes. The authors would also like to thank Prof. Peter HAYES for providing feedback on publication drafts, and to Dr Jeff CHEN for helping us in translating the abstract from English to Standard Chinese. Additionally, financial support from industrial sponsors Aurubis AG (Germany), the Australian Research Council Linkage Program, Boliden (Sweden), Metso Outotec Oyj (Finland), Nyrstar (Australia), Kazzinc Ltd, Glencore (Kazakhstan), and Umicore NV (Belgium) are gratefully acknowledged.

Supplementary Materials

Supplementary Materials in this paper can be found at: http://tnmsc.csu.edu.cn/download/18-p2183-2022-0380-Supplementary_Materials.pdf.

References

[1] FLORES G A, RISOPATRON C, PEASE J. Processing of complex materials in the copper industry: Challenges and opportunities ahead [J]. JOM, 2020, 72: 3447−3461.

[2] LENNARTSSON A, ENGSTRÖM F, SAMUELSSON C, BJÖRKMAN B, PETTERSSON J. Large-scale WEEE recycling integrated in an ore-based Cu-extraction system [J]. Journal of Sustainable Metallurgy, 2018, 4: 222−232.

[3] HAYES P C, SCHLESINGER M E, STEIL H U, SIEGMUND A. Lead smelter survey [C]//Lead−Zinc 2010 Symposium, Held in Conjunction with COM 2010. Vancouver: John Wiley & Sons, 2010: 345−413.

[4] MOATS M S, FILZWIESER A, WANG S, DAVENPORT W G, SIEGMUND A, ROBINSON T. Global survey of copper electrorefining: 2019 world tankhouse operating data [C]//Copper 2019. Vancouver: Metallurgy and Materials Society of CIM, 2019: 594940.

[5] JAK E, DECTEROV S A, HAYES P C, PELTON A D. Thermodynamic modelling of the system PbO−ZnO−FeO−Fe_2O_3−CaO−SiO_2 for zinc/lead smelting [C]//Proc 5th International Conference on Molten Slags, Fluxes and Salts. Sydney: Iron and Steel Society of AIME, 1997: 621−628.

[6] SHEVCHENKO M, JAK E. Experimental phase equilibria studies of the Pb−Fe−O system in air, in equilibrium with metallic lead and at intermediate oxygen potentials [J]. Metallurgical and Materials Transactions B, 2017, 48: 2970−2983.

[7] SHEVCHENKO M, JAK E. Thermodynamic optimization of the PbO−FeO−Fe_2O_3−SiO_2 system [J]. Calphad, 2019, 67: 101670.

[8] GEBHARDT E, OBROWSKI W. The ternary system copper−lead−oxygen [J]. Zeitschrift für Metallkunde, 1954, 45: 332−338.

[9] HOFMANN W, KOHLMEYER J. The system copper−lead−oxygen [J]. Zeitschrift für Metallkunde, 1954, 45: 339−341.

[10] SZILLAT H, TESKE C L. Synthesis and structure of the first ternary lead(II) copper(I) oxide: $PbCu_2O_2$ [J]. Zeitschrift für Anorganische und Allgemeine Chemie, 1994, 620: 1307−1311.

[11] CANCAREVIC M, ZINKEVICH M, ALDINGER F. Enthalpy of formation of Cu_2PbO_2 and revision of the

Cu_2O−PbO phase diagram [J]. Materials Science Forum, 2005, 494: 67−72.

[12] SHEVCHENKO M, JAK E. Experimental liquidus studies of the binary Pb−Cu−O and ternary Pb−Cu−Si−O systems in equilibrium with metallic Pb−Cu alloys [J]. Journal of Phase Equilibria and Diffusion, 2019, 40: 671−685.

[13] SHEVCHENKO M, JAK E. Thermodynamic optimization of the binary PbO−"Cu_2O", "Cu_2O"−SiO_2 and ternary PbO−"Cu_2O"−SiO_2 systems [J]. Calphad, 2020, 69: 318−326.

[14] YAZAWA A, EGUCHI M. Equilibrium studies on copper slags used in continuous converting [C]//YANNOPOULOS J C, AGARWAL J C. Extractive Metallurgy of Copper. Warrendale, PA: TMS, 1976: 3−20.

[15] TAKEDA Y. Phase diagram of CaO−FeO−Cu_2O slag under copper saturation [C]//Yazawa International Symposium: Metallurgical and Materials Processing: Principles and Techologies; Materials Processing Fundamentals and New Technologies. Minerals, Warrendale, PA: Metals & Materials Society, 2003: 211−225.

[16] ILYUSHECHKIN A, HAYES PC, JAK E. Liquidus temperatures in calcium ferrite slags in equilibrium with molten copper [J]. Metallurgical and Materials Transactions B, 2004, 35: 203−215.

[17] NIKOLIC S, HAYES P C, JAK E. Liquidus temperatures in the "Cu_2O"−FeO−Fe_2O_3−CaO system at molten metallic copper saturation [J]. Metallurgical and Materials Transactions B, 2009, 40: 900−909.

[18] HIDAYAT T, SHISHIN D, DECTEROV S, JAK E. Critical assessment and thermodynamic modeling of the Cu−Fe−O−Si system [J]. Calphad, 2017, 58: 101−114.

[19] JAK E, HAYES P C, LEE H G. Improved methodologies for the determination of high temperature phase equilibria [J]. Korean Journal of Minerals and Materials Institute (Seoul), 1995, 1: 1−8.

[20] JAK E. Phase equilibria to characterise lead/zinc smelting slags and sinters (PbO−ZnO−CaO−SiO_2− Fe_2O_3−FeO) [D]. University of Queensland, 1995.

[21] PHILIBERT J. Method for calculating the absorption correction in electron-probe microanalysis [C]//3rd International Symposium on X-Ray Optics and X-Ray Microanalysis. Stanford, CA: Stanford University, 1963: 379−392.

[22] DUNCUMB P, REED S J B. Calculation of stopping power and backscatter effects in electron probe microanalysis [R]. Cambridge: Tube Investments Research Laboratory, 1968: 133−154.

[23] DUNCUMB P. Quantitative electron probe microanalysis [C]//Proc 25th Anniversary Meeting of the Electron Microscopy Analysis Group. Cambridge: Institute of Physics and the Physical Society. Electron Microscopy and Analysis Group, 1971: 132−137.

[24] YAZAWA A. Distribution of various elements between copper, matte and slag [J]. Erzmetall, 1980, 33: 377−382.

[25] NIKOLIC S, HAYES P C, JAK E. Experimental techniques for investigating calcium ferrite slags at metallic copper saturation and application to the systems "Cu_2O"−"Fe_2O_3" and "Cu_2O"−CaO at metallic copper saturation [J]. Metallurgical and Materials Transactions B, 2009, 40: 892−899.

[26] LLOVET X, PINARD P T, DONOVAN J J, SALVAT F. Secondary fluorescence in electron probe microanalysis of material couples [J]. Journal of Physics D: Applied Physics, 2012, 45: 225301.

[27] SHEVCHENKO M, JAK E. Experimental liquidus studies of the Pb−Fe−Si−O system in air [J]. Journal of Phase Equilibria and Diffusion, 2019, 40: 319−355.

[28] SHEVCHENKO M, JAK E. Experimental liquidus studies of the Zn−Fe−Si−O system in air [J]. International Journal of Materials Research, 2019, 110: 600−607.

[29] KAWASAKI T, ISHIZUKA H. Experimental study of Fe^{3+} solubility in cristobalite and its application to a metamorphosed quartz-magnetite rock from Mt. Riiser-Larsen area, Napier Complex, East Antarctica [J]. Journal of Mineralogical and Petrological Sciences, 2008, 103: 255−265.

[30] BALE C W, BELISLE E, CHARTRAND P, DECTEROV S A, ERIKSSON G, GHERIBI A E, HACK K, JUNG I H, KANG Y B, MELANCON J, PELTON A D, PETERSEN S, ROBELIN C, SANGSTER J, SPENCER P, van ENDE M A. FactSage thermochemical software and databases, 2010—2016 [J]. Calphad, 2016, 54: 35−53.

[31] PELTON A D, CHARTRAND P. The modified quasichemical model. II — Multicomponent solutions [J]. Metallurgical and Materials Transactions A, 2001, 32: 1355−1360.

[32] PELTON A D, DECTEROV S A, ERIKSSON G, ROBELIN C, DESSUREAULT Y. The modified quasichemical model. I — Binary solutions [J]. Metallurgical and Materials Transactions B, 2000, 31: 651−659.

[33] CHARTRAND P, PELTON A D. On the choice of "Geometric" thermodynamic models [J]. Journal of Phase Equilibria, 2000, 21: 141−147.

[34] PELTON A D. A General "Geometric" thermodynamic model for multicomponent solutions [J]. Calphad, 2001, 25: 319−328.

[35] RISOLD D, NAGATA J I, SUZUKI R O. Thermodynamic description of the Pb−O system [J]. Journal of Phase Equilibria, 1998, 19: 213−233.

[36] SCHORNE-PINTO J, CASSAYRE L, PRESMANES L, BARNABÉ A. Insights on the stability and cationic nonstoichiometry of $CuFeO_2$ delafossite [J]. Inorganic Chemistry, 2019, 58: 6431−6444.

[37] JAK E, DECTEROV S A, WU P, HAYES P C, PELTON A D. Thermodynamic optimisation of the systems PbO−SiO_2, PbO−ZnO, ZnO−SiO_2 and PbO−ZnO−SiO_2 [J]. Metallurgical and Materials Transactions B, 1997, 28: 1011−1018.

[38] SHISHIN D, PROSTAKOVA V, JAK E, DECTEROV S. Critical assessment and thermodynamic modeling of the Al−Fe−O system [J]. Metallurgical and Materials Transactions B, 2016, 47: 397−424.

[39] SHISHIN D, HIDAYAT T, JAK E, DECTEROV S. Critical assessment and thermodynamic modeling of Cu−Fe−O system [J]. Calphad, 2013, 41: 160−179.

[40] MAH A D, PANKRATZ L B, WELLER W W, KING E G. Thermodynamic data for cuprous and cupric oxides [R]. Washington, DC: U.S. Department of the Interior, Bureau of Mines, 1967.

[41] STEBBINS J F, CARMICHAEL O S E, MORET L K. Heat capacities and entropies of silicate liquids and glasses [J]. Contributions to Mineralogy and Petrology, 1984, 86: 131−148.

[42] RICHET P. Heat capacity of silicate glasses [J]. Chemical Geology, 1987, 62: 11−124.

[43] LANGE R A, NAVROTSKY A. Heat capacities of iron(3+) oxide-bearing silicate liquids [J]. Contributions to Mineralogy and Petrology, 1992, 110: 311−320.

[44] STILLINGER F H. Supercooled liquids, glass transitions, and the Kauzmann paradox [J]. Journal of Chemical Physics, 1988, 88: 7818−7825.

[45] MISHRA R K, DUBEY K S. Thermodynamic behavior of undercooled melts [J]. Bulletin of Materials Science, 1996, 19: 357−371.

[46] JOHARI G P. An equilibrium supercooled liquid's entropy and enthalpy in the Kauzmann and the third law extrapolations, and a proposed experimental resolution [J]. Journal of Chemical Physics, 2000, 113: 751−761.

[47] SPEEDY R J. Kauzmann's paradox and the glass transition [J]. Biophysical Chemistry, 2003, 105: 411−420.

[48] TAKEDA K, MIYAKE K, HITAKA M, KAWAE T, YAGUCHI N, MEKATA M. Thermal analysis of freedom of spin in partially disordered state of the antiferromagnetic triangular lattice in $CuFeO_2$ [J]. Journal of the Physical Society of Japan, 1994, 63: 2017−2020.

[49] MITSUDA S, MASE M, UNO T, KITAZAWA H, KATORI H A. H-T magnetic phase diagram of a frustrated triangular lattice antiferromagnet $CuFeO_2$ [J]. Journal of the Physical Society of Japan, 2000, 69: 33−36.

[50] PETRENKO OA, BALAKRISHNAN G, LEES MR, MCK PAUL D, HOSER A. High magnetic field behavior of the triangular lattice antiferromagnet, $CuFeO_2$ [J]. Physical Review B, 2000, 62: 8983−8988.

[51] BARANY R, PANKRATZ L B, WELLER W W. Thermodynamic properties of cuprous and cupric ferrites [R]. Washington, DC: U.S. Department of the Interior, Bureau of Mines, 1964.

[52] ROSENQVIST T, HOFSETH A. Phase relations and thermodynamics of the copper−iron−sulfur−oxygen system at 700−1000 °C [J]. Scandinavian Journal of Metallurgy, 1980, 9: 129−138.

[53] ERIKSSON G, TEGMAN R. Thermodynamic studies of high temperature equilibriums. XVII: Determination of the stability of copper ferrate ($CuFe_2O_4$) by EMF measurements using stabilized zirconium as solid electrolyte [J]. Chemica Scripta, 1976, 10: 145−148.

[54] JACOB K T, FITZNER K, ALCOCK C B. Activities in the spinel solid solution, phase equilibriums and thermodynamic properties of ternary phases in the system copper−iron−oxygen [J]. Metallurgical and Materials Transactions B, 1977, 8B: 451−460.

[55] ZINOVIK MA. Conditions for the existence of copper−nickel ferrospinels and phase equilibriums during their reduction [J]. Zhurnal Neorganicheskoi Khimii (Журнал неорганической химии), 1988, 33: 738−742. (in Russian)

[56] PAULSSON H, ROSEN E, TEGMAN R. Thermodynamic studies of high temperature equilibria. XIII: Potentiometric determination of the stability of copper iron oxide ($CuFeO_2$) using a galvanic cell involving stabilized zirconium oxide as solid electrolyte [J]. Chemica Scripta, 1975, 8: 193−196.

[57] FLOYD J M, WILLIS G M. Phase relations and oxygen dissociation pressures in the system Cu−Fe−O [C]//WOODCOCK J T, JENKINS A F, WILLIS G M. Research in Chemical and Extraction Metallurgy. Melbourne: Australasian Institute of Mineralogy and Metallurgy, 1967: Monograph Series No. 2: 61−64.

[58] ZALAZINSKII A G, BALAKIREV V F, CHEBOTAEV N M, CHUFAROV G I. Thermodynamic analysis of the reduction, dissociation, and formation of copper aluminate, copper chromate(III), and copper ferrate(II) from the free elements and oxides [J]. Zhurnal Neorganicheskoi Khimii (Журнал неорганической химии), 1969, 14: 624−626. (in Russian)

[59] ONO K, IMAMURA Y, YAMAGUCHI A, MORIYAMA J. Equilibrium phase diagram of the iron−copper−oxygen system [J]. Nippon Kinzoku Gakkaishi, 1972, 36: 701−704.

[60] FREDRIKSSON M, ROSEN E. Thermodynamic studies of high temperature equilibriums. XIV: On phase relations and equilibrium oxygen pressures in the system copper−copper ferrate−iron(III) oxide−iron(II,III) oxide at temperatures 1100−1300 K [J]. Chemica Scripta, 1976, 9: 118−121.

[61] SCHMAHL N G, MULLER F. Equilibriums in the system copper−iron−oxygen [J]. Archiv für das Eisenhüttenwesen, 1964, 35: 527−532.

[62] SCHAEFER S C, HUNDLEY G L, BLOCK F E, MCCUNE R A, MRAZEK R V. Phase equilibriums and X-ray diffraction investigation of the system copper−iron−oxygen [J]. Metallurgical Transactions, 1970: 2557−2563.

[63] KATKOV A E, LYKASOV A A. Spinel phase relations in the Fe_3O_4−$CuFe_2O_4$ system [J]. Inorganic Materials, 2003, 39: 171−174.

[64] SPENCER H M, SPICER W M. The heat capacities of red and yellow lead monoxides at high temperatures [J]. Journal of the American Chemical Society, 1942, 64: 617−621.

[65] KING E G. Low temperature heat capacities and entropies at 298.15°K. of lead sesquioxide and red and yellow lead monoxide [J]. Journal of the American Chemical Society, 1958, 80: 2400−2401.

[66] KOSTRYUKOV V N, MOROZOVA G K. Thermodynamic study at low temperatures. X: Heat capacity of yellow modification of lead oxide in the temperature range from 12.5 to 303 K. and the entropy at 298.15 K [J]. Russian Journal of Physical Chemistry, 1960, 34: 873−874.

[67] KNACKE O, PRESCHER K E. Thermodynamische messungern an bleioxid [J]. Zeitschrift für Erzbergbau und Metallhüttenwesen, 1964, 17: 28−34.

[68] KOSTRYUKOV V N, SAMORUKOV O P, SAMORUKOVA N K, NURULLAYEV N G. The entropy of tin oxide(II) and lead oxide(II) at 298.15 K [R]. All-Union Institute for Scientific and Technical Information (Academy of Sciences USSR), 1977: 4458−4477.

[69] KOBERTZ D. Vaporization and caloric studies on yellow lead oxide PbO [J]. Calphad, 2019, 65: 155−164.

[70] HIDAYAT T, SHISHIN D, JAK E, DECTEROV S. Thermodynamic reevaluation of the Fe−O system [J]. Calphad, 2015, 48: 131−144.

[71] COUGHLIN J P, KING E G, BONNICKSON K R. High-temperature heat contents of ferrous oxide, magnetite and

ferric oxide [J]. Journal of the American Chemical Society, 1951, 73: 3891−3893.

[72] GRØNVOLD F, STØLEN S, TOLMACH P, WESTRUM EFJ. Heat capacities of the Wustites $Fe_{0.9379}O$ and $Fe_{0.9254}O$ at temperatures T from 5 K to 350 K. Thermodynamics of the reaction: xFe(s)+(1/4)Fe_3O_4(s)=$Fe_{0.7500}$+xO(s)=$Fe_{1-y}O$(s) at T=850 K, and properties of $Fe_{1-y}O$(s) to T=1000 K. Thermodynamics of formation of wustite [J]. Journal of Chemical Thermodynamics, 1993, 25: 1089−1117.

[73] STOLEN S, GLOCKNER R, GRONVOLD F, ATAKE T, IZUMISAWA S. Heat capacity and thermodynamic properties of nearly stoichiometric Wustite from 13 to 450 K [J]. American Mineralogist, 1996, 81: 973−981.

[74] GRØNVOLD F, WESTRUM E F. α-ferric oxide: Low temperature heat capacity and thermodynamic functions [J]. Journal of the American Chemical Society, 1959, 81: 1780−1783.

[75] HU J H, JOHNSTON H L. Low temperature heat capacities of inorganic solids. IX: Heat capacity and thermodynamic properties of cuprous oxide from 14 to 300 °C [J]. Journal of the American Chemical Society, 1951, 73: 4550−4551.

[76] GREGOR L V. The heat capacity of cuprous oxide from 2.8 to 21 °C [J]. The Journal of Physical Chemistry, 1962, 66: 1645−1647.

[77] SHISHIN D, DECTEROV S A. Critical assessment and thermodynamic modeling of Cu−O and Cu−O−S systems [J]. Calphad, 2012, 38: 59−70.

[78] HAYES F H, LUKAS H L, EFFENBERG G, PETZOW G. A thermodynamic optimization of the copper−silver−lead system [J]. Zeitschrift für Metallkunde, 1986, 77: 749−754.

[79] HIDAYAT T, SHISHIN D, DECTEROV S A, JAK E. Experimental study and thermodynamic re-evaluation of the FeO−Fe_2O_3−SiO_2 system [J]. Journal of Phase Equilibria and Diffusion, 2017, 38: 477−492.

PbO−“$CuO_{0.5}$”和 PbO−“$CuO_{0.5}$”−“$FeO_{1.5}$”渣体系与金属相平衡的实验和热力学建模

X. WEN, M. SHEVCHENKO, E. JAK

Pyrometallurgy Innovation Centre (PYROSEARCH), School of Chemical Engineering,
The University of Queensland, Brisbane, QLD 4072, Australia

摘　要：为了支撑现有以及新兴火法冶金工艺的改进和研发，作为 PbO−ZnO−Cu_2O−FeO−Fe_2O_3−CaO−SiO_2−Al_2O_3−MgO−S−(微量 As, Sn, Sb, Bi, Ag, Au, Ni, Cr 和 Co)19 种元素多组分渣/锍/合金/黄渣系统热力学研究的一部分，对 PbO−“CuO0.5”和 PbO−“$CuO_{0.5}$”−“$FeO_{1.5}$”体系在金属铜以及铅铜合金饱合条件下的相平衡进行研究。试样采用高温平衡加淬火处理，并使用电子探针(EPMA)直接测量渣相、固体氧化物相和金属相的成分以确定体系的相平衡。通过实验获得铅黄(PbO)、尖晶石($(Fe,Cu)Fe_2O_4$)、赤铜矿(Cu_2O)、铁氧体铅($Pb_{2+x}Fe_2O_{5+x}$)、磁铁铅矿($Pb_{1+x}Fe_{12-x}O_{19-x}$)、铜铅矿($Cu_2PbO_2$)和赤铜铁矿($CuFeO_2$)在 688~1000 ℃的初晶相区相平衡广数据。PbO−“CuO0.5”系统的实验结果表明，铜铅矿(Cu_2PbO_2)发生不一致熔化，而非如之前的研究表明它在低于二元共晶温度的情况下分解形成铅黄(PbO)和赤铜矿(Cu_2O)。基于过去和现在的实验研究结果，采用 FactSage 热力学计算软件包导出一组描述系统中所有物相的自洽热力学模型参数。

关键词：氧化铅；氧化铜；氧化铁；相图；液相线；渣；金属；相平衡

(Edited by Bing YANG)